ORIGINAL PAPER



Middle to late Holocene paleolimnology of a sinkhole lake in the northern Bahamas and its linkage to regional climate variability

Anne E. Tamalavage · Peter J. van Hengstum · Sarah J. Feakins · Shawna N. Little · Sloan Coats · Tyler S. Winkler · Richard M. Sullivan · Patrick Louchouarn · Jeffrey P. Donnelly · Nancy A. Albury

Received: 2 December 2022 / Accepted: 7 June 2023 / Published online: 29 August 2023 © The Author(s), under exclusive licence to Springer Nature B.V. 2023

Abstract Sinkholes develop on carbonate landscapes when caves collapse and can subsequently become lake-like environments if they are flooded by local groundwater. Sediment cores retrieved from sinkholes have yielded high-resolution reconstructions of past environmental change, hydroclimate, and hurricane activity. However, our understanding of the internal sedimentary processes of these systems remains incomplete. Here, we use a multiproxy approach including sedimentology (stratigraphy, coarse-grained particle density, bulk organic matter content), micropaleontology (ostracods), and geochemistry (δ^{13} C and δ^{2} H on *n*-alkanoic acids) to reconstruct evidence for paleolimnology and regional hydroclimate from a continuous stratigraphic record (Emerald Pond sinkhole) in the northern Bahamas that spans the middle to late Holocene. Basal peat at 8.9 m below modern sea level documents the maximum sea-level position at ~8200 cal. yr BP. Subsequent upward vertical migration of the local aquifer caused by regional sea-level rise promoted carbonate-marl deposition from ~8300 to 1700 cal. yr BP. A shift in coarse particle deposition and ostracods at 5500 cal. yr BP suggests some environmental change, which may be related to one or multiple internal or external drivers. Sapropel deposition from ~1700 to 1300 cal. yr BP indicates a fundamental change in limnology to promote increased organic matter preservation, perhaps related to the regional cooling during the Dark Ages Cold Period. We find $\delta^2 H_{28}$ values are largely invariant from 7700 to 6150 cal. yr BP suggesting a generally stable hydroclimate (mean

A. E. Tamalavage (⊠)

Department of Biological Sciences, Université de Montréal, Montréal, QC, Canada e-mail: anne.tamalavage@umontreal.ca

A. E. Tamalavage \cdot P. J. van Hengstum \cdot T. S. Winkler \cdot R. M. Sullivan

Department of Oceanography, Texas A&M University, College Station, TX, USA

P. J. van Hengstum

Department of Coastal and Environmental Science, Texas A&M University at Galveston, Galveston, TX, USA

S. J. Feakins

Department of Earth Sciences, University of Southern California, Los Angeles, CA, USA S. N. Little

Department of Marine Biology, Texas A&M University at Galveston, Galveston, TX, USA

S. Coats

Department of Earth Sciences, University of Hawaii, Honolulu, HI, USA

T. S. Winkler · J. P. Donnelly

Department of Geology and Geophysics, Woods Hole Oceanographic Institution, Woods Hole, MA, USA

P. Louchouarn

School of Earth Sciences, The Ohio State University, Columbus, OH, USA

N. A. Albury

Coastal Cave Survey, West Branch, IA, USA



-133%, $1\sigma = 5\%$). The shift to more depleted values (-156%, $1\sigma = 19\%$) at $\sim 6000-4800$ cal. yr BP may be linked to a weakened (eastern displaced) North Atlantic Subtropical High. Nevertheless, additional local hydroclimate records are needed to better disentangle uncertainties from either internal or external influences on the resultant measurements.

Keywords Coastal sinkhole lakes · Holocene hydroclimate · Leaf-wax geochemistry · Carbonate sedimentology

Introduction

Across the Lucayan (Bahamian) archipelago (The Bahamas and Turks and Caicos Islands), stratigraphic successions that are temporally continuous with a high sedimentation rate that span the middle (~8200-4200 cal. yr BP) to late (4200 cal. yr BP to present) Holocene are rare. Recoverable stratigraphy is commonly less than 3 m in most inland ponds and marine lagoons, and the temporal duration is typically limited to the late Holocene when sedimentation was initiated by sea-level rise flooding depressions on the antecedent carbonate surface (Dix et al. 1999; Mackinnon and Jones 2001; Noble et al. 1995; Park 2012; Rasmussen et al. 1990; Teeter 1995). These successions are also frequently bioturbated, which limits their application to addressing paleoclimate questions. While speleothems are a common target for developing paleoclimate records on carbonate landscapes (Arienzo et al. 2017; Fensterer et al. 2013), not all low-lying carbonate islands have the caves and speleothems necessary to assess climate variability in the subtropical North Atlantic. Additional environmental records are required to fully understand the more localized impacts of climate and land-use change in the region (Steadman et al. 2014).

Alternatively, the stratigraphy, geochemistry and environmental proxies preserved in sinkhole and karst lakes can provide insight into regional hydroclimate and landscape dynamics (Fall et al. 2021; Gabriel et al. 2009; Gregory et al. 2017; Grimm et al. 1993; Kjellmark 1996; Peros et al. 2017; Tamalavage et al. 2020; Wallace et al. 2019; Winkler et al. 2020). Sinkholes develop after a cave collapses on the carbonate platform (Cole 1910; Mylroie et al. 1995a, b; Park Boush et al. 2014), and they can provide space

for the long-term accumulation of undisturbed sedimentary records. This geomorphologic setting is a dynamic environment that is controlled by both (a) linkages between groundwater vertical elevation and regional sea level, and (b) linkages between groundwater hydrodynamics and local hydroclimate (Gabriel et al. 2009; Gregory et al. 2017; Shinn et al. 1996; van Hengstum et al. 2011, 2018, 2020a). Environmental development in sinkholes during inundation from a transgressive sea-level cycle can be briefly summarized into the following stages: (1) wetland colonization and peat deposition caused by sea-level inundation, (2) development of palustrine-lacustrine settings as vertical migration of the coastal aquifer floods the basin with a freshwater meteoric lens, (3) onset of meromictic conditions as vertical migration of the coastal aquifer continues, causing both an upper meteoric lens and lower saline water mass to be positioned within the sinkhole, and finally (4) a proximal shoreline position and eventual inundation by sea level which promotes fully marine conditions. During stage two (above), sinkholes and lakes on carbonate landscapes can be flooded by well-oxygenated groundwater that is typically carbonate-saturated, promoting lacustrine marl accumulation, which in turn provides a stratigraphic target to explore for evidence of changing groundwater conditions related to regional changes in water balance (evaporationprecipitation; Holmes 1998; Peros et al. 2017; Street-Perrott et al. 1993).

In January 2006, a near-continuous and high-resolution stratigraphic succession spanning the middle to late Holocene was recovered from a sinkhole known as Emerald Pond on Abaco Island within the Little Bahama Bank (Slayton 2010). The stratigraphy was primarily lacustrine marl, and the preserved pollen-based evidence documented middle to late Holocene terrestrial ecological changes. However, the detailed stratigraphy in Emerald Pond also presents an opportunity to investigate long-term groundwater hydrologic variability, potentially in response to changing regional hydroclimate. Elsewhere in the western tropical North Atlantic, the middle to late Holocene is punctuated by multiple megadroughts (Hodell et al. 1991a, 1995, 2001, 2005; Lane et al. 2014, 2009), yet records in the Bahamian Archipelago are scarce. While annual rainfall in the Yucatan region is strongly overprinted by seasonal migrations of the Intertropical Convergence Zone (ITCZ; Haug



et al. 2001), rainfall along the western tropical north Atlantic margin has multiple confounding influences. For example, western boundary displacements of the North Atlantic Subtropical High (NASH) strongly influence rainfall in boreal summer, and the El Niño/Southern Oscillation (ENSO) impacts boreal winter rainfall (Gamble and Curtis 2008; Jury et al. 2007; Li et al. 2012).

Here we provide a detailed examination of the paleolimnology and environmental changes preserved in Emerald Pond through (i) stratigraphic analysis and radiocarbon dating of additional sediment cores, (ii) benthic meiofaunal remains (e.g., ostracods and testate amoebae) as a long-term hydrographic indicator, and (iii) evidence for local hydroclimate change using geochemical changes in terrestrial plant wax.

Study site

Abaco Island lies on the eastern margin of the Little Bahama Bank (26.79°N, 77.42°W; Fig. 1), which is the northernmost carbonate platform in the Bahamian (Lucayan) Archipelago (Carew and Mylroie 1997; Walker et al. 2008) once inhabited by the indigenous Lucayan people. Sinkholes and other karst features are ubiquitous on the Bahamian landscape (Mylroie 1995; Whitaker and Smart 1997). Tropical hardwoods and palms covered the Abaco landscape until ~700 years ago when pine trees (*Pinus caribaea* var. *bahamensis*) first became dominant as humans (Lucayans) transformed the landscape into a firedominated system (Fall et al. 2021; Slayton 2010).

Emerald Pond is currently a shallow (<4 m), groundwater-fed sinkhole that is located 1.8 km inland from the eastern shore of Great Abaco. Emerald Pond is ~ 26 m in diameter with a ~ 4 m limestone cliff between the surrounding carbonate surface and water table in the sinkhole (Fig. 1). In unconfined carbonate aquifers, sinkholes essentially function as uncased wells, and the vertical physicochemical conditions of sinkhole water columns can reflect the local aquifer's hydrographic structure. If deep enough, terrestrial sinkholes can have a tripartite water-column structure: an upper meteoric lens (fresh to slightly oligohaline), a transitional mixing zone or pycnocline, and basal saline groundwater (van Hengstum et al. 2016, 2018, 2020a). As defined and applied by others (Beddows et al. 2007; Little et al. 2021), the mixing zone is the layer separating isohaline and isothermal values.

The groundwater level varies in response to the tidal range which is ~1 m measured at Pelican Harbor Tide Gauge (Abaco Island, https://tidesandcurrents.noaa.gov/). This range is common in unconfined coastal aquifers (Coutino et al. 2021; Little and van Hengstum 2019; Martin et al. 2012). Presently, no significant quantities of aquatic macrophytes like *Chara* occur in the sinkhole, but algae covers the sediment-water interface. There is little bathymetric variability, yet water depth modestly increases around the sinkhole perimeter. No significant cave passages extend from the sinkhole into the phreatic zone, but there is a small overhang (<2 m) on one side.

Since there is no long-term instrumental record of rainfall on Abaco Island, the compilation of Jury et al. (2007) provides a surrogate for regional hydroclimate. Based on the Nassau rain gauge (~170 km south of Emerald Pond) spanning from 1855 CE to present, mean annual rainfall (MAR) in the Abaco Island area is $\sim 1470 \text{ mm yr}^{-1}$, with $\sim 75\%$ of annual rainfall occurring during the wet season (May-October; Fig. 2a), and ~25% occurring in the dry season from November to April (~50 mm month⁻¹). The closest station with measured rainfall isotopic data is "Centro de Protección e Higiene de la Radiación" (IAEA/WMO 2019), Havana in Cuba (Fig. 2b). Weighted mean annual $\delta^2 H$ is -11.8% (wet season mean $\delta^2 H - 15.2\%$, dry season mean $\delta^2 H - 3.5\%$). Local rainfall amount and isotopic composition is highly sensitive to strength (central pressure) and geographic positioning (westward margin) of the NASH (Li et al. 2011, 2012), especially during boreal summer. Regional-to-large scale climate dynamics associated with local variability in δ^2 H can be simulated with the isotope-enabled Community Earth System Model (iCESM; Tamalavage et al. 2020). During the most ²H-enriched (²H-depleted) years, the NASH is intensified (weakened) and expanded westward (displaced to the northeast from Abaco), the Caribbean Low Level Jet (CLLJ) is strengthened (weakened), which causes suppressed (enhanced) convection and rainfall over the Caribbean. This is similar to the factors that impact large scale hydroclimate dynamics across the Mesoamerican-Caribbean region (Bhattacharya and Coats 2020).



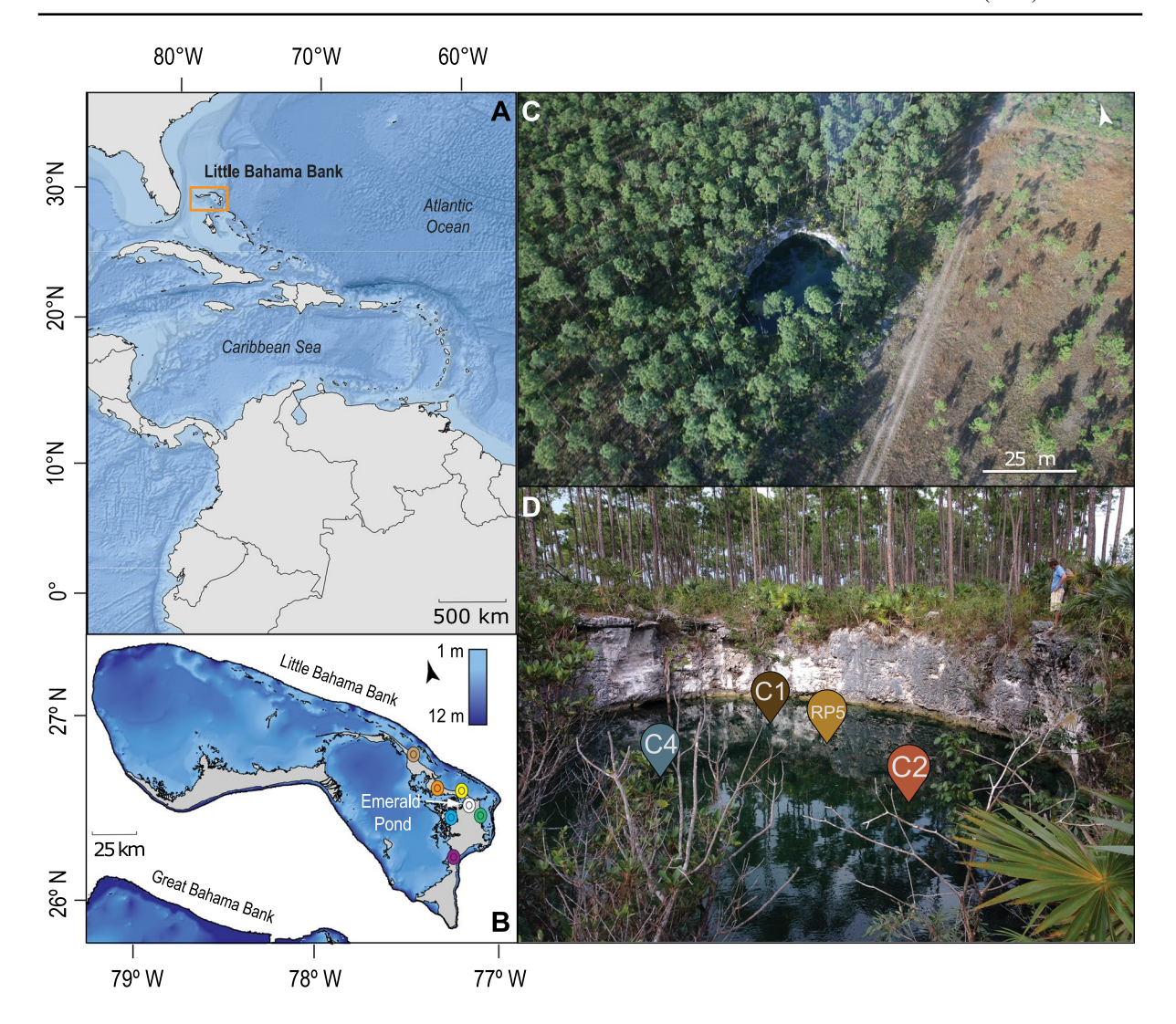


Fig. 1 A Tropical North Atlantic with the Little Bahama Bank outlined in orange, adapted from (Sullivan et al. 2021), **B** Scaled in photo of the Little Bahama bank, with Emerald Pond (26.54° N, –77.11W) sinkhole shown in white, plus other sinkhole basins on Abaco with paleoenvironmental records including: Blackwood sinkhole (brown), No Man's Land (orange),

Great Cistern (yellow), Runway (green), Freshwater River blue hole (blue), and Sawmill Sink (purple), C Aerial photo of Emerald Pond (photo by Nancy Albury), D Landscape-level photo of Emerald Pond (photo by Nancy Albury) with coring locations marked

Methods

Fieldwork

The shallow water depth and small size of Emerald Pond allowed the sediment-water interface to be extensively observed by snorkelers prior to sediment coring, and the shallow subsurface was explored with probes. Hand-driven push cores easily penetrated the sediment and a layer of pine needles was found,

which created an obstacle for further push coring. However, vibracores were collected in 2016 (EMLD C1, C2, C4) using 7.6-cm diameter aluminum pipes that were fitted with a polycarbonate-core catcher at the pipe base (i.e., core nose) to enhance the likelihood of recovering unlithified sediments. Additionally, a push core was recovered in December 2018 (EMLD RP5) to sample the upper~1 m. Core RP5 was recovered with a 7.6-cm diameter polycarbonate pipe without a core catcher, and suction was created



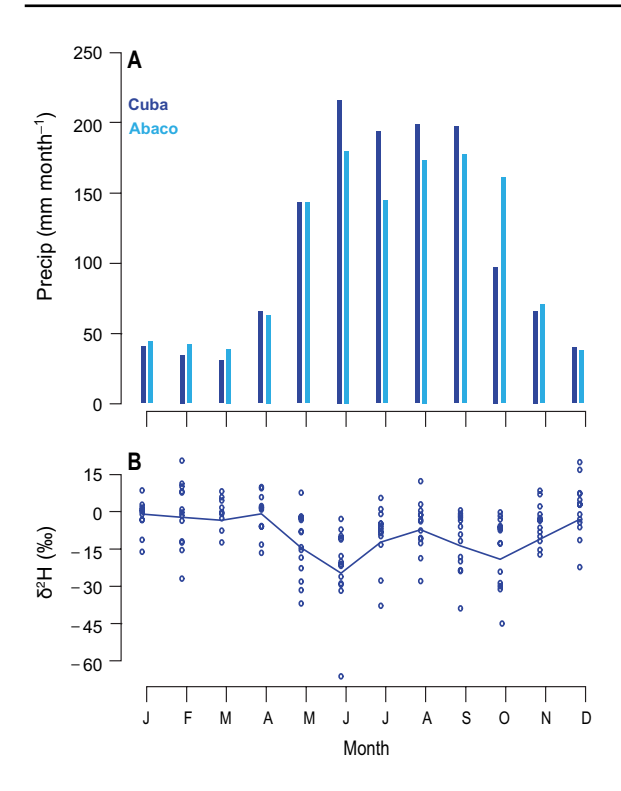


Fig. 2 A Monthly mean precipitation from "Centro de Protección e Higiene de la Radiación", Havana, Cuba (dark blue) and the Nassau, Bahamas (light blue) rain gauge (1855–2017), adapted from (Sullivan et al. 2021), **B** Measured mean (line) and individual values (dots) within the respective month, showing range of $\delta^2 H_{precip}$ from Centro de "Centro de Protección e Higiene de la Radiación"

for sediment sampling with a rubber-test plug. This offers the best opportunity to carefully collect the uppermost stratigraphy near the sediment-water interface. Immediately after coring, and while the pipe was still positioned vertically in the water column, floral foam was manually inserted into the core pipe to stabilize the sediment-water interface during core extraction and subsequent transport.

Depth-wise hydrographic profiles were collected in multiple seasons spanning several years (June 2016, January 2017, January 2018, July 2018, and July 2019) to better characterize water column variability. Temperature (± 0.01 °C), salinity (± 0.1 psu), pH (± 0.1 pH units), dissolved oxygen (± 0.1 mg L⁻¹), and depth (± 0.004 m) were measured using a YSI EXO1 multiparameter sonde, with a data-sampling rate of 2 Hz. The sonde was routinely calibrated before deployment, and the pH sensor was replaced annually before fieldwork to promote accuracy in

field measurements. Salinity was calculated from conductivity and temperature readings using instrument calibrations for the YSI EXO1, using algorithms found in Standard Methods for the Examination of Water and Wastewater (American Public Health Association 1989; in reference to the conductivity of standard seawater at 15 °C).

Lithology and chronology

In the laboratory, all cores were split lengthwise, photographed, X-rayed, and stored at 4 °C until further analysis. The coarse sediment content in the stratigraphy (>63 μm) was contiguously measured downcore using the Sieve-First Loss-on-Ignition (Sieve-First LOI) procedure (van Hengstum et al. 2016) at 1-cm increments for EMLD C1, C2, C4 and RP5. Samples were first wet-sieved over a 63 µm mesh, dried for 12 h in an oven at 80 °C and weighed to determine the sediment mass. The residual coarse fractions were then combusted for 4 h at 550 °C in a muffle furnace to remove sedimentary organic matter (OM), with the choice of temperature selection based on experiments by Heiri et al. (2001). Samples were then re-weighed post-combustion to determine inorganic mass. The variability in coarse sediment fraction was then expressed as mass per unit volume (D > 63 µm mg cm⁻³). A paired 1.25 cm³ sub-sample, also taken contiguously downcore at 1-cm intervals, was used for LOI following standard methods (550 °C, 4.5 h) to determine bulk OM content, reported as weight percent (%) of the original sediment mass (Heiri et al. 2001). Analytical uncertainty on replicate Sieve First and standard LOI measurements is typically less than $\pm 1\%$. Coarse sedimentary particles (>63 µm in diameter) were qualitatively examined wet in Petri dishes using stereomicroscopes. Six samples were selected within the homogeneous carbonate marl to determine general mineralogy with X-ray diffraction (XRD) analysis, measured on a Bruker-AXS D8 Advanced Bragg-Brentano X-ray powder diffractometer using standard protocols. Minerals were determined in each sample by comparing diffractograms with the 2005 International Center for Diffraction Data (ICDD) material identification database.

Terrestrial plant macrofossils (n=30) were radiocarbon dated at the National Ocean Sciences Accelerator Mass Spectrometry facility at Woods Hole Oceanographic Institution to generate downcore-age



models and calculate sedimentation rates (Table 1). The conventional radiocarbon age results were calibrated into calendar years before present (cal. yr BP) with IntCal20 using 1950 CE as present (Reimer et al. 2020). The final downcore Bayesian age model for EMLD C1, C2, C4 and RP5 was computed with Bacon (v2.5.1) in R Studio. This output provides probability estimates at each designated level downcore (Blaauw and Christen 2011), and we calculated age outputs for every contiguous cm downcore.

Microfossil analyses

Lacustrine marl sediments from EMLD C1, C2, and C4 were subjected to detailed microfossil analysis for benthic meiofauna (small benthic invertebrates). Ostracods were the dominant meiofaunal remains preserved in the sediments, with no benthic foraminifera observed aside from a few occurrences (<5 individuals total). A separate 0.63 cm³ sediment subsample was obtained from the cores at ~50-year intervals, based on calculated Bacon-age models, and wet-sieved over a 125 µm mesh to concentrate ostracod valves. Given the low taxonomic diversity, a census of 120 valves per sample was sought at each stratigraphic level. In some instances, additional sediment was subsampled to meet minimum census goals. However, it was less common for samples to have excessive valve numbers that required sub-splitting into aliquots. All taxonomic identifications were completed to species level and by the same researcher to limit individual bias on the results, and taxonomy was verified with a Hitachi TM3000 scanning electron microscope and appropriate literature (Furtos 1936; Keyser 1975, 1977; Keyser and Schöning 2000; Krutak 1971; Pérez et al. 2010b; Swain 1955; Teeter 1980, 1995; Van Morkhoven 1963). In total, 258 samples comprised the final microfossil database for all cores, containing six different ostracod species. The downcore ostracod-census taxa were ultimately divided into timewise assemblages based on the change in dominant taxa. Only six taxonomic categories were observed in the ostracods, and through many stratigraphic levels, only one or two taxa represented > 80% of the sample. Given the strong dominance of few taxonomic categories, the final ostracod assemblages were qualitatively defined based on changes in the dominant taxa.

The total count of charophyte gyrogonites and testate amoebae were evaluated as additional paleoenvironmental indicators. Charophyte 'stoneworts' are benthic green macroalgae that are common in hard-water lakes, and their gyrogonites are well-preserved in the stratigraphy of carbonate lakes in both the modern and fossil record (Soulié-Märsche 2008; Soulié-Märsche and García 2015). The dried sediment subsamples from all cores were analyzed for charophyte gyrogonites in the sieved>125 µm size fraction simultaneously with the ostracods and tallied as individuals per cm³. In addition, the total concentration of testate amoeba (individuals > 45 µm in size per cm³) were enumerated. Most testate amoebae are benthic single-celled organisms that are known to prefer well-oxygenated bottom conditions with salinities typically < 3.5 psu (Escobar et al. 2008; Roe and Patterson 2006; van Hengstum et al. 2008).

n-Alkanoic acid abundance and isotopic analyses

Sediment samples (~1 g) were collected for biomarker analysis every 10 cm downcore from EMLD C4, with additional samples added to increase resolution (n=110). Within RP5, samples were taken at consistent \sim 5-cm intervals (n = 12). Samples were freeze-dried and homogenized with a mortar and pestle. Methods for lipid extraction, purification, methylation, and quantification were identical to those reported for a nearby sinkhole (Tamalavage et al. 2020). Briefly, n-alkanoic acids (prepared as fatty acid methyl esters, FAMEs) were identified by gas chromatography mass spectrometry (GC-MS). FAMEs were quantified for all 110 samples by flame ionization detection (FID) relative to an in-house standard comprising a mixture of 3 n-alkanoic acid methyl esters of known concentration.

Compound-specific hydrogen isotopic (δ^2 H) and carbon isotopic (δ^{13} C) compositions were determined by gas chromatography isotope ratio mass spectrometry (GC-IRMS) for n=29 and n=12 samples, respectively (as repeat isotopic analyses are destructive, not all samples had sufficient residual to be measured for both). We used a Thermo Scientific Trace gas chromatograph equipped with a Rxi-5 ms column (30 m×0.25 mm, film thickness 0.25 µm) and a programmable temperature vaporization (PTV) injector operated in solvent split mode with an evaporation temperature of 60 °C. The GC was connected



via a GC Isolink with pyrolysis furnace (at 1400 °C for hydrogen) or a combustion oven (at 1000 °C for carbon) to a Conflo IV interface to a DeltaV + isotope ratio mass spectrometer. To check for hydrogen linearity (across 1-8 V), the H_3^+ factor was measured daily and remained close to 4 ppm mV⁻¹. For carbon, the standard deviation of reference pulses was better than 0.9%. Reference peaks of H2 or CO2 were co-injected during the course of a GC-IRMS run and used for standardization. Data were normalized to the VSMOW/SLAP hydrogen isotopic scale by comparing with an external standard run several times per day (A3 mix for samples run before August 2017; A6 mix for samples run after August 2017). Standards were obtained from A. Schimmelmann (Indiana University) and contained 15 n-alkane compounds $(C_{16}-C_{30})$, with δ^2 H values spanning – 46 to – 227‰; and δ^{13} C values spanning – 33.37 to – 28.61% for A3 mix and -33.97 to -26.15% for A6 mix. The RMS error determined by replicate standard measurements during analyses was 3.7% for δ^2 H and 0.21% δ^{13} C. Correction for H or C added by methylation of fatty acids as methyl esters was made by way of mass balance (Lee et al. 2017). The results are reported using conventional delta notation (δ^2 H and δ^{13} C in permil, %o),

$$\delta = ((R_{\text{sample}} - R_{\text{standard}}) / R_{\text{standard}}) \times 1000$$
 (1)

in which R is 2 H/ 1 H or 13 C/ 12 C, respectively. In order to reconstruct the isotopic composition of precipitation, we applied the net fractionations ($\varepsilon_{28/\text{precip}}$) of -121% ($\pm 3\%$) reported for C_{28} *n*-alkanoic acids within tropical forests (Feakins et al. 2016) to calculate δ^2 H_{precip}.

Results

Modern water column structure

The hydrographic profiles collected over multiple years indicate that vertical water-column conditions are seasonally dynamic (Fig. 3). However, stratified water layers are not easily defined within Emerald Pond. For example, profiles taken in June 2016, January 2018, and July 2018 measured a relatively isothermal water column (variability < 1 °C), with higher temperatures (~28 °C) observed in the entire

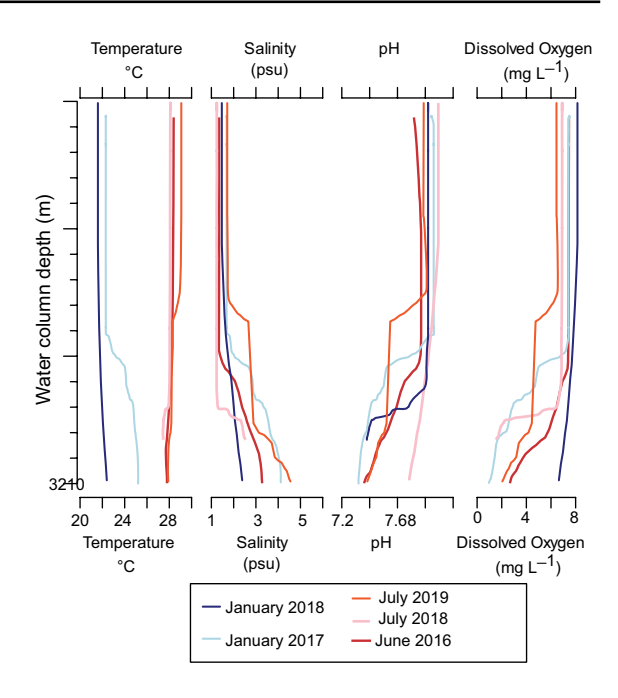


Fig. 3 Hydrographic depth profiles from Emerald Pond, Little Bahama Bank. Data collected with a YSI EXO1 multiparameter sonde

water column during boreal summer. The greatest vertical temperature variability (~4 °C) and a defined thermocline were observed in January 2017. Although all measured salinities are within the oligohaline range (0.5-3.5 psu), a subtle halocline was observed in June 2016, January 2017, July 2018, and July 2019. Surface salinities of the meteoric lens ranged from 1.2 to 1.6 psu, and the depth at which salinity started to change was variable (e.g., 1.8 m in January 2017 versus 2.2 m in July 2018). pH values in the meteoric lens ranged from 7.5 to 7.9 (mean: 7.8 ± 0.04), decreasing along salinity (density) gradients to values ~ 0.3 pH less than surface measurements. Dissolved oxygen concentration in the meteoric lens ranges from 6.3 to 8.4 mg L^{-1} , with decreasing concentration with depth along physicochemical gradients. In general, lower dissolved oxygen concentrations were observed during the summer. At the sediment-water interface, which is ~ 3 m depth across most of the flat-bottomed sinkhole lake, the mean dissolved oxygen concentration was 0.4-5.4 mg L⁻¹ (highest concentration during January 2018 profile), ranging from dysoxic to oxic conditions. The data indicate that Emerald Pond was flooded by the meteoric lens of the local unconfined aquifer in the



carbonate platform. However, hydrographic conditions are sensitive to seasonal changes in atmospheric conditions, which contribute to the shallow water column (~3 m), narrow diameter (~26 m), limited internal water volume, proximity of the water table to the subaerial landscape (~4 m cliff), variability in groundwater chemistry, and direct freshwater additions through rainfall or evaporation, and impact salinity at the sediment-water interface.

Age model and sediment stratigraphy

All coring efforts terminated at a consistent subsurface elevation, and basal recovered sediment was medium to coarse carbonate gravel and fragments (e.g., EMLD C4; Fig. 4A). The four cores retrieved from Emerald Pond recorded different temporal ranges based on age-model results (Fig. 5). EMLD RP5 spanned~1900-1300 cal. yr BP, EMLD C1~5200-2300 cal. yr BP, EMLD C2~8000-3400 C2 cal. yr BP, and EMLD C4~8300–2600 cal. yr BP. EMLD C4 was the longest stratigraphic succession, while EMLD C1 and RP5 recorded the most recent sediments. Three primary facies characterize the middle-to-late Holocene stratigraphy in Emerald Pond: (i) basal peat from ~8350 to 8290 cal. yr BP, (ii) lacustrine carbonate marl from ~8290 to 1700 cal. yr BP, and (iii) sapropel from ~1700 to 1300 cal. yr BP. Bulk coarse carbonate particles and bulk OM content varied throughout the facies (Appendix A, Table 2).

Immediately above the carbonate fragments 8.9 m below the water table, a peat deposit was recovered within EMLD C4. Similar basal sediment was previously encountered (Slayton 2010), and this suggests full recovery of the available unlithified stratigraphy preserved in Emerald Pond. The peat deposit had a bulk OM content exceeding 75%, and it contained fibrous leaf and wood fragments in a fine-grained organic-rich matrix. The presence of fibrous OM and low concentrations of mangrove pollen (Slayton 2010) within the peat deposit at Emerald pond suggest wetland taxa growing in situ. Terrestrial plant macrofossils (fibrous organic material) from the peat deposit base were dated to 8230 cal. yr BP (1σ range: 8260-8200 cal yr. BP), which provided a minimum onset age for peat deposition. However, suitable conditions for peat accumulation at the bottom of the sinkhole were short lived.

The stratigraphy indicated that carbonate marl accumulated in Emerald Pond from~8300 to 1700 cal. vr BP, but with a variable sedimentation rate. Carbonate marl deposition began at ~ 8285 cal. yr BP (1σ range: 8250–8320 cal yr. BP) in EMLD C4, though this is slightly older than the basal age for carbonate marl deposition at EMLD C2 (8070 ± 50 cal. yr BP; Fig. 6). The shorter EMLD C1 only sampled lacustrine marl that was younger than 5150 ± 20 cal. yr BP. However, a notable coarse-grained gastropod-shell layer (Planborbis, Fig. 4e) could be correlated between EMLD C1 at 210 cm and EMLD C2 at 90 cm, which were dated to 3780 ± 30 and 3780 ± 10 cal. yr BP, respectively (Fig. 6). EMLD C1 successfully sampled lacustrine marl that was deposited from ~5150 to 2320 cal. yr BP. The overall sedimentation rate within the lacustrine marl unit in EMLD C4 was similar to EMLD C2 (1.2 cm yr⁻¹). However, the sedimentation rate at the site of EMLD C1 (~5200-2260 cal. yr BP) and EMLD RP5 (47–60 cm) was lower, 0.9 cm yr⁻¹ and 0.6 cm yr⁻¹, respectively. EMLD C2 and C4 did not recover any sediment younger than ~ 3200 cal. yr BP and ~2700 cal. yr BP, respectively. We think this was caused by sampling interference from a pine needle layer in the shallow surface—this layer acted as a barrier and prevented the core catcher in the aluminum pipe (i.e., core nose) to engage and sample the less consolidated sediment in the upper stratigraphy. As such, core sampling did not actually initiate until older (> 3000-year-old) and more compacted carbonate sediment was penetrated by the core pipe. The RP5 push core sampled a carbonate marl and sapropel contact dated to $\sim 1720 \pm 15$ cal. yr BP (Fig. 7), which indicated when carbonate marl deposition had ceased in Emerald Pond.

The carbonate marl had a fine-grained carbonate-mineral matrix, which is interspersed with gastropods and terrestrial OM fragments (e.g., pine needles, bark, leaf fragments). XRD analysis indicated that the marl is primarily high-loaded Mg-bearing calcite. Bulk OM was uniform and consistent throughout the unit (mean: 6±9%, range: 1.3–86%), but distinctive organic-rich laminations occurred just above the basal peat (Fig. 4C). Radiographs documented continuous laminations throughout the carbonate marl, which suggests negligible bioturbation (Fig. 4D). There were organic-rich, green-hued intervals that occur only from ~8140 to 6000 cal. yr BP (EMLD



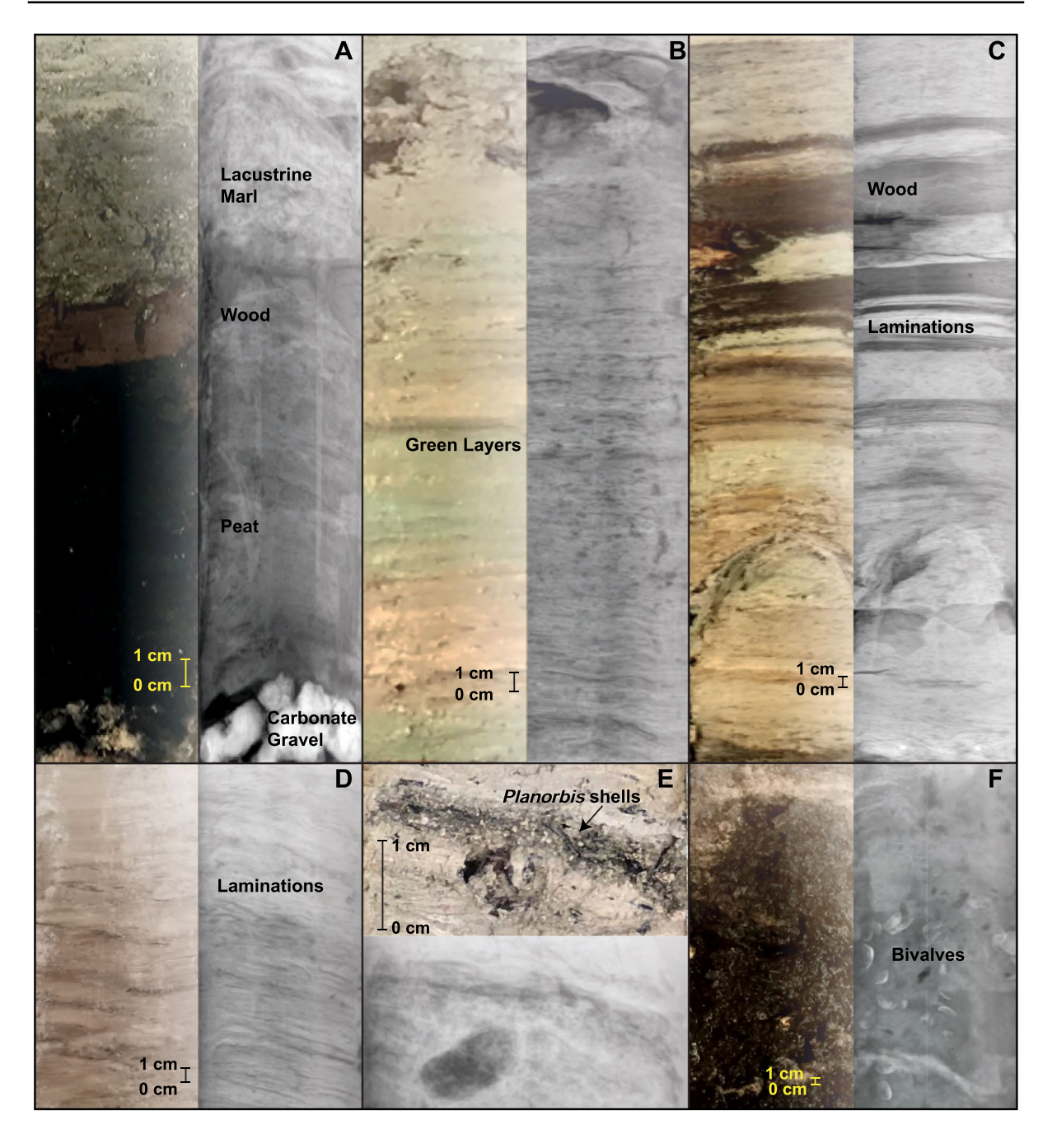


Fig. 4 Photographs and radiographs of selected sections of the studied cores in Emerald Pond, Little Bahama Bank (see Fig. 2), **A** 690–716 cm of EMLD C4 showing basal peat to lacustrine marl transition, **B** 510–540 cm of EMLD C2 showing green layers, **C** 605–670 cm of the basal stratigraphy

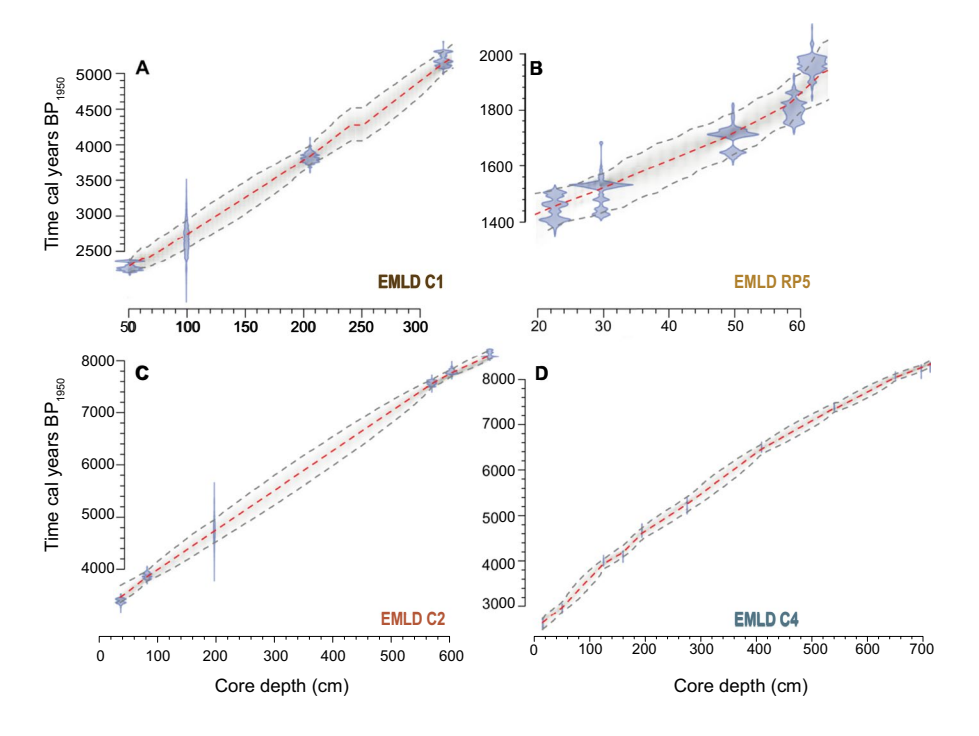
C2: 430–660 cm, EMLD C4: 440–690 cm; Fig. 6), and they were not associated with a salient textural change (Fig. 4B). It is likely that green-hued intervals

of EMLD C2, **D** 40–60 cm of EMLD C2 showing homogenous carbonate mud with laminae, **E** coarse grained deposit at \sim 208 cm in EMLD C1, and **F** sapropel layer in EMLD C5 from 7 to 26 cm with abundant bivalves visible in the x radiograph

are from preserved remains of blue-green algae in the sedimentary matrix, which thrive in shallow, coastal carbonate environments (Black 1932).



Fig. 5 Bayesian age-depth models for all cores collected in Emerald Pond, Little Bahama Bank. Models were developed using Bacon (v2.5.1) in R. Dated substrates (blue shaded shapes) are terrestrial macrofossils (Appendix A, Table 1), gray dashed lines bind the minimum and maximum 95% confidence interval around possible model age-depth outputs, with the red line representing the 'best' model based on the mean age for each depth (Blaauw and Christen 2011)



The most interesting textural characteristics were the consistent trends in coarse sedimentary particle deposition between EMLD C2 and C4, and the striking loss of coarse particle deposition in the last 5000 years (Appendix A Table 2, Fig. 6). In general, there was more coarse particle content and variability from~8200 to~5200 cal. yr BP (e.g., EMLD C4, mean: $117.8 \ \mu m \ cm^{-3}$, range: $19.1-264.0 \ \mu m$ cm⁻³), which thereafter abruptly decreased (mean values from 117.8 to 56.1 μm cm⁻³). Stereomicroscopic examination of 13 downcore sub-samples from EMLD C2, including analysis of layers with both increased (> 140 mg cm⁻³) and decreased coarse fraction content (< 50 mg cm⁻³), indicated that individual coarse particles are most likely derived from within the sinkhole itself. Ostracods and biogenic calcite structures (calcite tubes and circular particles; Fig. 6) dominated the > 63 µm particle fraction, but the quantity of individual constituents varied. Calcite-tube structures have been described from other carbonate lakes, and they are thought to be autogenic calcite precipitation around submerged vegetation or aquatic algae from increased pH related to primary productivity (Leng et al. 2010; Pełechaty et al. 2013). More modest differences in coarse particle deposition between EMLD C2 and C4 from~7100 to 5200 cal.

yr BP likely reflects site-specific conditions at coring locations.

The youngest sedimentary deposits preserved in Emerald Pond are the sapropel in EMLD RP5 and organic-rich sediment in EMLD C1. The upper 50 cm of EMLD RP5 is dark brown-hued, biogenic sapropel with some coarse-grained OM particles (e.g., some stem fragments). Sapropel is a fine-grained OM deposit typically comprised of decomposed algal, bacterial, or higher plant sources (Schnurrenberger et al. 2003). Mean bulk OM within the sapropel unit of EMLD RP5 (10–45 cm) was $62.2 \pm 14.3\%$ (Fig. 7), which is an order of magnitude higher than the carbonate marl (mean: $5.7 \pm 8.1\%$). During qualitative assessment, a few ostracod valves were observed in the sapropel (Candona annae, Cytheridella ilosvayi) but testate amoebae were absent. The upper part of the sapropel also contained a high concentration of intact bivalve shells not observed elsewhere in the stratigraphy, but it cannot be assumed that these infauna organisms are syndepositional with the sapropel. Based on the radiocarbon date at 49.5 cm (1720 \pm 10 cal. yr BP) in EMLD RP5, the sapropel started to accumulate ~ 1700 cal. yr BP. The time when sapropel was accumulating in RP5 (~1720 to~1300 cal. yr BP) was consistent with the decrease in sedimentation



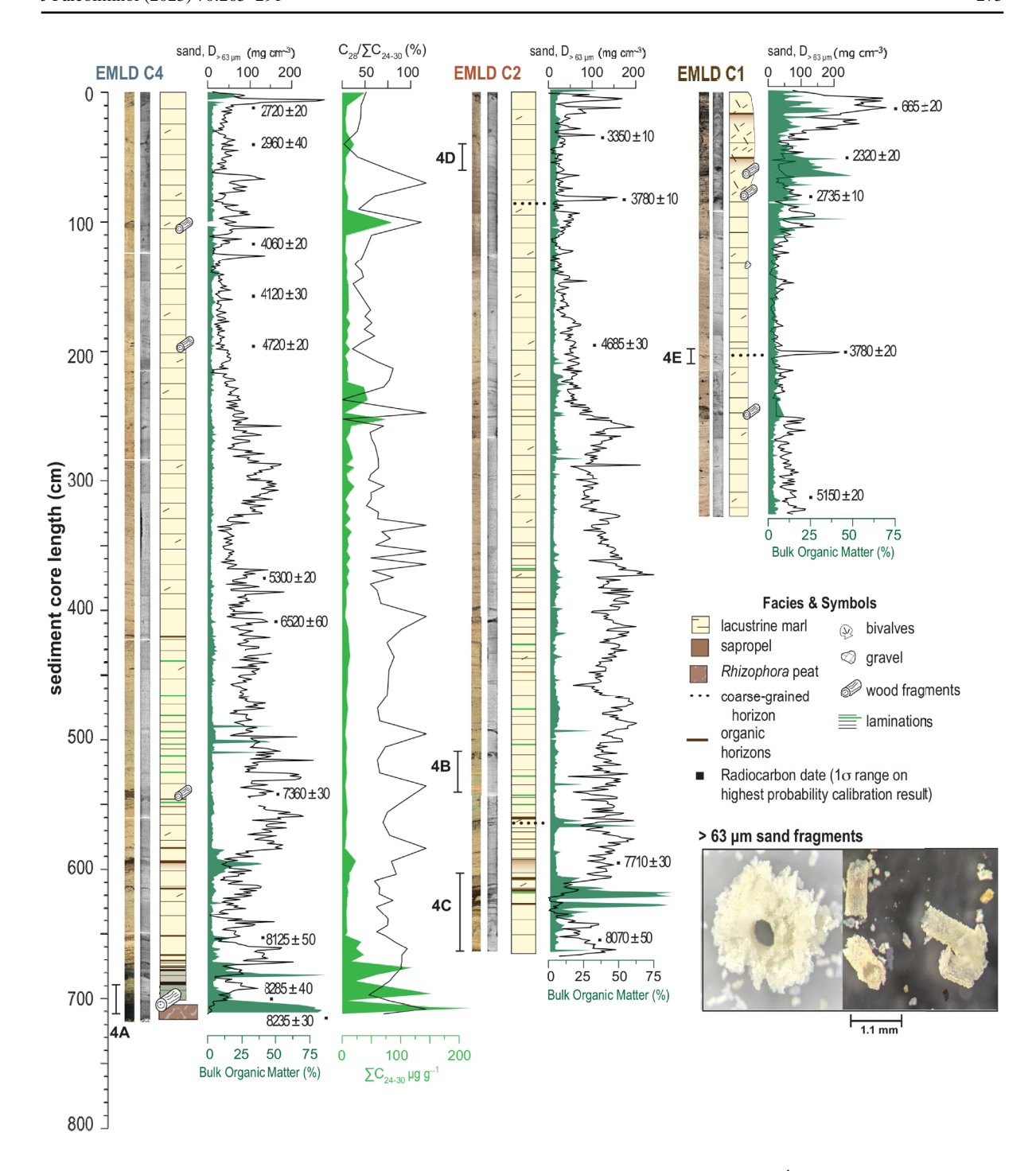


Fig. 6 Stratigraphic columns and radiocarbon dates from cores EMLD C1, C2 and C4, Emerald Pond, Little Bahama Bank. Selected, bracketed sections (e.g., 4A on EMLD C4) correspond with images in Fig. 4. Downcore coarse-grained particle deposition (Sieve-First LOI, D > 63 μ m), bulk organic matter (dark green, classic LOI, weight %), sum of n-alkanoic

acids (light green) C_{24-30} (µg g^{-1}) for EMLD C4, and relative abundance of matter (dark green, classic LOI, weight %), sum of n-alkanoic acids (light green) $C2_{24-30}$ (µg g^{-1}) for EMLD C4, and relative abundance of C28 n-alkanoic acid (%) for EMLD C4 are plotted



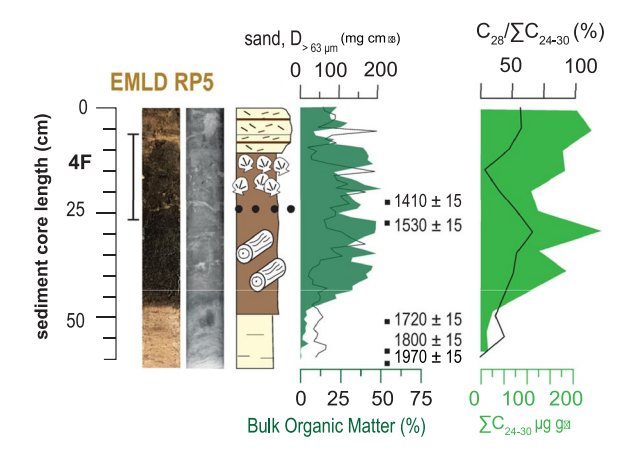


Fig. 7 Stratigraphy and radiocarbon dates for core EMLD RP5, Emerald Pond, Little Bahama Bank. Selected, bracketed sections (e.g., 4F on EMLD RP5) correspond with images in Fig. 4. Downcore coarse-grained particle deposition (Sieve-First loss-on-ignition (LOI), D > 63 μ m) mg cm⁻³, bulk organic matter (dark green, LOI, weight %), sum of *n*-alkanoic acids (light green) C₂₄₋₃₀ (μ g g⁻¹), and relative abundance of C₂₈ *n*-alkanoic acid (%) are plotted for RP5. Legend as in Fig. 6

rates and higher OM% observed in the top 50 cm of EMLD C1, which spanned the last millennium. This assumes that the radiocarbon date from 10.5 cm in EMLD C1 (665 ± 20 cal. yr BP) accurately reflects its stratigraphic age. The upper 50 cm in Emerald Pond spanned the last ~2000 years, with RP5 indicating that conditions suitable for sapropel deposition likely ceased just before 1310 cal. yr BP.

Ostracod assemblages, charophytes and testate amoebae

In general, ostracod remains were well preserved with valve density ranging from 21 to 6209 valves cm⁻³, and the assemblages dominated by low diversity groupings (species richness range: 2–6). The six observed species of ostracode are: *Candona annae* (Méhes 1914), *Cyprideis americana* (Sharpe 1908), *Cypridopsis vidua* (Müller 1776), *Cytheridella ilosvayi* (Daday 1905), *Darwinula stevensoni* (Brady and Robertson 1870), and *Physocypria globulus* (Furtos 1933). The downcore changes in the relative abundance of all taxa follow the same broad changes in all cores with multi-decadal to centennial variability (Fig. 8). Variation between cores is most likely related to site-specific processes (e.g., slight changes

in bathymetry, water depth at deposition). From oldest to youngest, the ostracods were grouped into four assemblages that are described below.

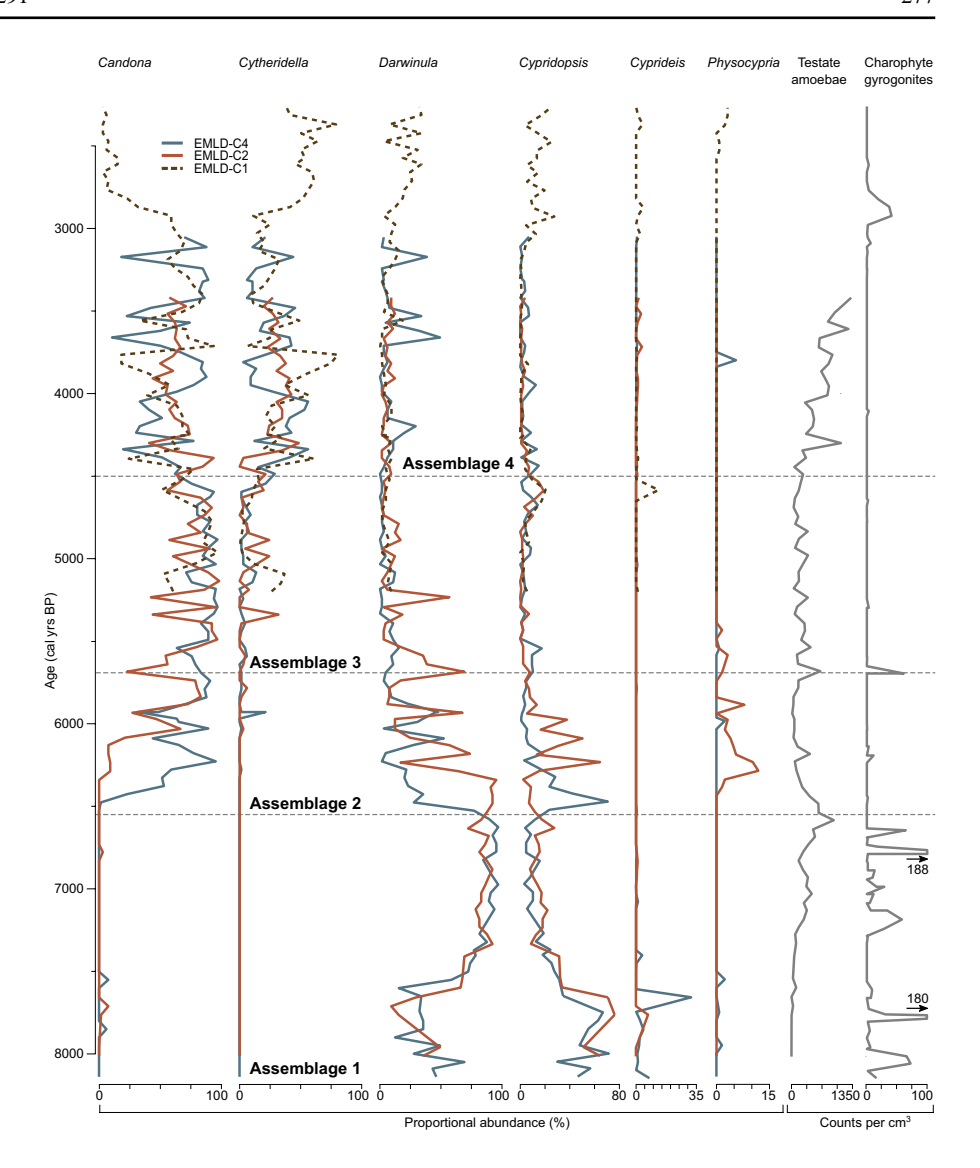
Assemblage 1 occurred from 8150 to 7600 cal. yr BP and is dominated by both Darwinula stevensoni (mean: 35.8%) and Cypridopsis vidua (mean: 59.9%). Assemblage 2 occurs from ~6400 to 7600 cal. yr BP and is dominated by D. stevensoni (mean: 82.2%), with lesser proportions of C. vidua (mean 16.7%). Darwinula stevensoni (freshwater biofacies) is a widespread taxon that prefers salinities less than 2 psu (Holmes 1997; Keyser 1977; Pérez et al. 2010a, 2010b). These taxa commonly co-occur in the fresh to slightly oligohaline subtropical and tropical waters in the Bahamas (Teeter 1989), Bermuda (Keyser and Schöning 2000), and south Florida (Keyser 1978). The gyrogonites of charophytes were most commonly observed within Assemblages 1 and 2, with gyrogonite remains having the highest density (gyrogonites cm^{-3}) from ~8100 to 5600 cal. yr BP. There are several large peaks of gyogonites (>60 gyrogonites cm⁻³) at 5700, 6800, 7800, and 8000 to 8050 cal. yr BP. After 5700 cal. yr BP, charophytes were absent from EMLD and did not consistently reappear except for a brief period from ~2950 to 2850 cal. yr BP.

Ostracod diversity slightly increases in assemblages 3 and 4, and preserved charophyte remains become negligible. Within Assemblage 3 (6400 to 4400 cal. yr BP), there was an overall decreasing relative abundance of D. stevensoni and C. vidua (samples with > 80% to 5–10%). At 4400 cal. yr BP, Candona annae colonized the sinkhole, and became the dominant ostracod in the community (mean: 70.5%). Candona annae is common in the shallow, oligohaline (<3 psu) environments of Florida, but it has been observed to tolerate salinities up to 6-8 psu (Keyser 1977). By 5500 cal. yr BP, Cytheridella ilosvayi increases in relative contribution to the assemblage, but still was generally < 5% of the assemblage. Cytheridella ilosvayi is a warm water taxon that is common throughout the tropics to subtropics (30°N-30°S). Assemblage 4 (4400 to 2200 cal. yr BP) was dominated by C. annae (mean: 53.5%), C. ilosvayi (mean: 31.5%), with less relative abundance of D. stevensoni (mean: 10%) and *C. vidua* (mean: 4.3%).

Testate amoebae (thecamoebians) were present in nearly all samples from EMLD C2, with an average density of 334 individuals cm⁻³ (range: 0 to 1319 cm⁻³). While initial sediment (peat) lacked testate



Fig. 8 Downcore abundances of ostracods, testate amoebae and charophytes in the studied cores from Emerald Pond, Little Bahama Bank



amoebae, test density quickly increased. The first major increase at ~7050 cal. yr BP was followed by a second, larger increase from 6800 to 6450 cal. yr BP. The numbers fluctuated until 164.5 cm when testate-amoebae densities began to consistently increase until the end of the EMLD C2 at 3400 cal. yr BP with the highest observed density of 1319 individuals cm⁻³. The presence of testate amoebae throughout the succession indicates that salinity did not exceed their ecological tolerance range (0–3.5 psu, van Hengstum et al. 2008) from the middle to late Holocene.

n-Alkanoic acid abundance

For biomarker analysis, each sample integrated 1 cm of stratigraphy, or ~8 years in EMLD C4 and ~9 years in EMLD RP5. As such, the final record has individual datapoints that average annual changes over about a decade (each 1 cm of sediment), with an observation about once a century (every 10 cm downcore). We found plant wax n-alkanoic acids with characteristic homologous series distributions typical of vascular, terrestrial plants (Freeman and Pancost 2014). Within EMLD C4, concentrations of n-alkanoic acids with chain lengths of 24 (0.4–59 μ g g⁻¹), 26 (0.4–40.6 μ g g⁻¹), 28 (0.2–216.9 μ g g⁻¹) and 30 (0.2–57.5 μ g g⁻¹) were quantified. Concentrations of



 C_{28} decline after ~4800 cal. yr BP (with some samples < ~1 µg g⁻¹). Overall, the modal chain length of *n*-alkanoic acids was 28, with an average chain length (ACL) of 27±0.8 (1 σ , n=105). The average carbon preference index (CPI) was 8.9±7. Both ACL and CPI indicate inputs from terrestrial higher plants

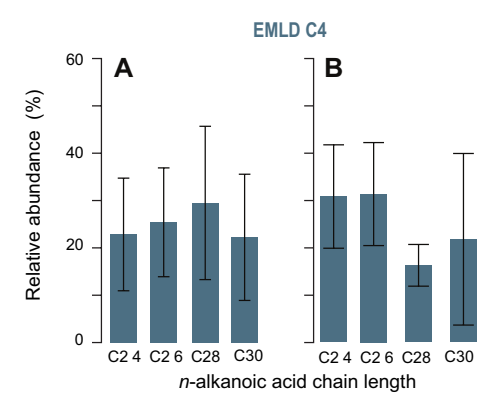


Fig. 9 Chain length abundance of *n*-alkanoic acids for whole EMLD C4 core (A) and the section from 0.5 to 213.5 cm (B) from Emerald Pond, Little Bahama Bank. In this core ~213 cm corresponds to a change in coarse-grained particle deposition (D>63 μ m)

(Freeman and Pancost 2014). Within EMLD RP5, n-alkanoic acids were quantified with carbon chain lengths of 24 (3.2–34.3 μ g g⁻¹), 26 (3.9–51.5 μ g g⁻¹), 28 (2.1–101.3 μ g g⁻¹) and 30 (1.6–58.1 μ g g⁻¹). The modal chain length was 28 with an ACL of 27 ± 0.5 (1 σ , n=12).

The sum of *n*-alkanoic acid concentrations (C₂₄₋₃₀) co-varies with bulk OM% (e.g., increase in \sum *n*-alkanoic acids with increased OM%) downcore in both EMLD C4 and RP5 (Figs. 6 and 7), providing evidence of continuous terrestrial OM input to Emerald Pond through time. There were two main patterns in chain length abundance in EMLD C4 from ~8300 to 4800 and ~4800 to 2650 cal. yr BP. C_{28} has a higher relative abundance $(C_{28}/\sum$ C_{24} : C_{30}) between 8320 and 4780 cal. yr BP (mean 30%), compared to 16% from 4780 to 2630 cal. yr BP (Fig. 9), and this higher abundance of C_{28} is synchronous with a decrease in > 63 µm particle density. The dominant C₂₈ n-alkanoic acid relative abundance from ~8300 to 4800 cal. yr BP is typical of tropical forests (Feakins et al. 2016). Although *n*-alkanoic chain lengths from C_{24} - C_{30} are common in land plants, C₂₄ and C₂₆ can also derive from

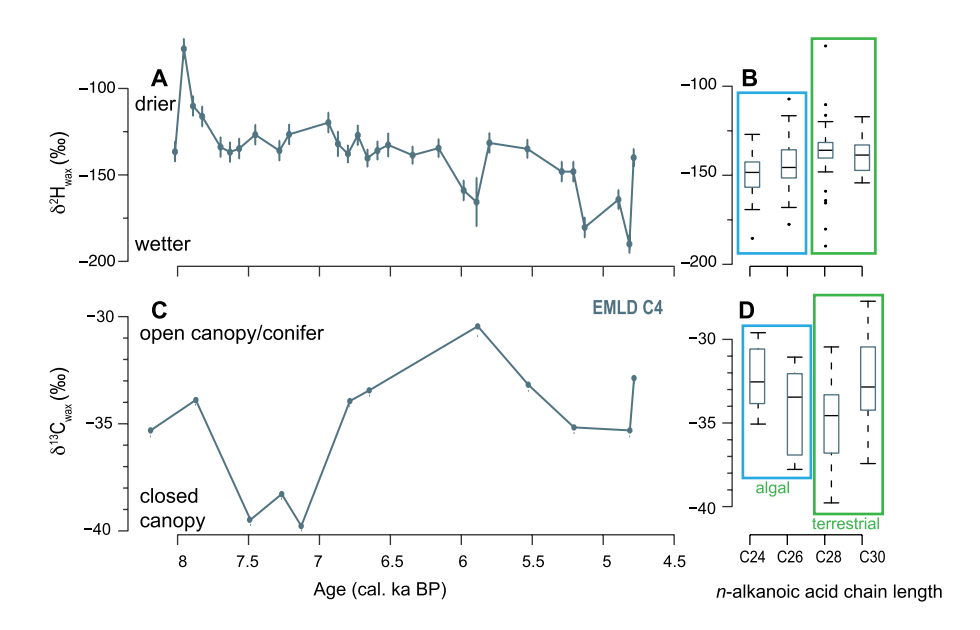


Fig. 10 Hydrogen isotopic measurements for *n*-alkanoic acids within core EMLD C4, Emerald Pond, Little Bahama Bank. **A** Downcore $\delta^2 H_{28}$ values for the mid-Holocene, **B** $\delta^2 H$ values by chain length for the even chain length C_{24} to C_{30} *n*-alkanoic acids, **C** Downcore $\delta^{13} C_{28}$ values, and D $\delta^{13} C$ values by chain length for the even chain length C_{24} to C_{30} *n*-alkanoic acids.

Box and whisker plots (**B**, **D**) show median (thick line), interquartile range (box), and range (whiskers). Based on abundance and isotopic composition, the C_{24} and C_{26} are thought to reflect aquatic production by algae (blue box) whereas the C_{28} and C_{30} *n*-alkanoic acids are likely derived from the leaf wax of land plants (green box)



submerged/floating aquatic macrophytes (Ficken et al. 2000). Therefore, the decrease in C_{28} *n*-alkanoic acid dominance (from 30 to 16% relative abundance) after ~4800 cal. yr BP and increased dominance of C_{26} (Fig. 10B) could be due to increased inputs from aquatic plants (Ficken et al. 2000), whereas we infer the C_{28} chain length derives from terrestrial plants.

Hydrogen and carbon isotopes

Unfortunately, the quantification work on all 110 samples indicated that the 1 g samples were [generally] insufficient for isotopic analyses presumably due to low plant-wax-accumulation rates and carbonate dilution. Only samples below 213.5 cm core depth in EMLD-C4 yielded sufficient C₂₈ n-alkanoic acid abundances for isotopic analyses (n=29 out of 110 samples studied). Hydrogen isotopic compositions of *n*-alkanoic acids from EMLD C4 ranged from – 186 to -127% (mean: -152%, $1\sigma = 12\%$, n = 38) for C_{24} , -178 to -107% (mean: -149%, $1\sigma = 15\%$, n=36) for C_{26} , -190 to -77% (mean: -138%), $1\sigma = 21\%$, n = 29) for C₂₈, and -154 to -117%(mean: $-138\%_0$, $1\sigma = 11\%_0$, n = 9) for C₃₀ (Fig. 10A). Values of $\delta^2 H_{28}$ span ~ 110% throughout the record. $\delta^2 H_{28}$ values were relatively stable from ~ 7680 to 6150 cal. yr BP (mean: -133, $1\sigma = 5\%$, n = 15), and are generally more depleted from ~5970 to 4780 cal. yr BP (mean: -156, $1\sigma = 19\%$, n = 10). Reconstructed $\delta^2 H_{precip}$ values from ~8320 to 4780 cal. yr BP ranged from -68 to 12% (mean: -22%), $1\sigma = 20\%$; Fig. 11B).

Carbon isotopic compositions of *n*-alkanoic acids from EMLD C4 ranged from -35 to -27% (mean: -32%₀, $1\sigma = 2\%$ ₀, n = 12) for C₂₄, -37 to -28%₀ (mean: -33%, $1\sigma = 3\%$, n = 12) for C_{26} , -39 to -30% (mean: -34%, $1\sigma = 3\%$, n = 12) for C_{28} , and -37 to -28% (mean: -33%, $1\sigma = 2\%$, n = 12) for C_{30} . $\delta^{13}C_{28}$ values were determined from a subset of 18 downcore samples from EMLD C4 (Fig. 10B). Values of $\delta^2 C_{28}$ ranged ~ 9% throughout the record. $\delta^{13}C_{28}$ values were most depleted from ~ 7600 to 7100 cal. yr BP (mean: $-39\%_0$, $1\sigma = 0.8\%_0$), aligned with values measured in late Holocene records from nearby Blackwood Sinkhole when pollen indicated there were abundant tropical hardwoods and palms on the landscape (Fall et al. 2021; Tamalavage et al. 2020). From~4200 to 2700 cal. yr BP, the low

concentrations of C_{28} (less than ~ 1 µg g⁻¹) made it difficult to obtain sufficient material for robust isotopic determinations in the processed samples. A larger sample mass (> 20 g) would be required to generate isotopic determinations consistently downcore. However, sediment availability is limited in narrow bore cores and larger samples equate to lower temporal resolution.

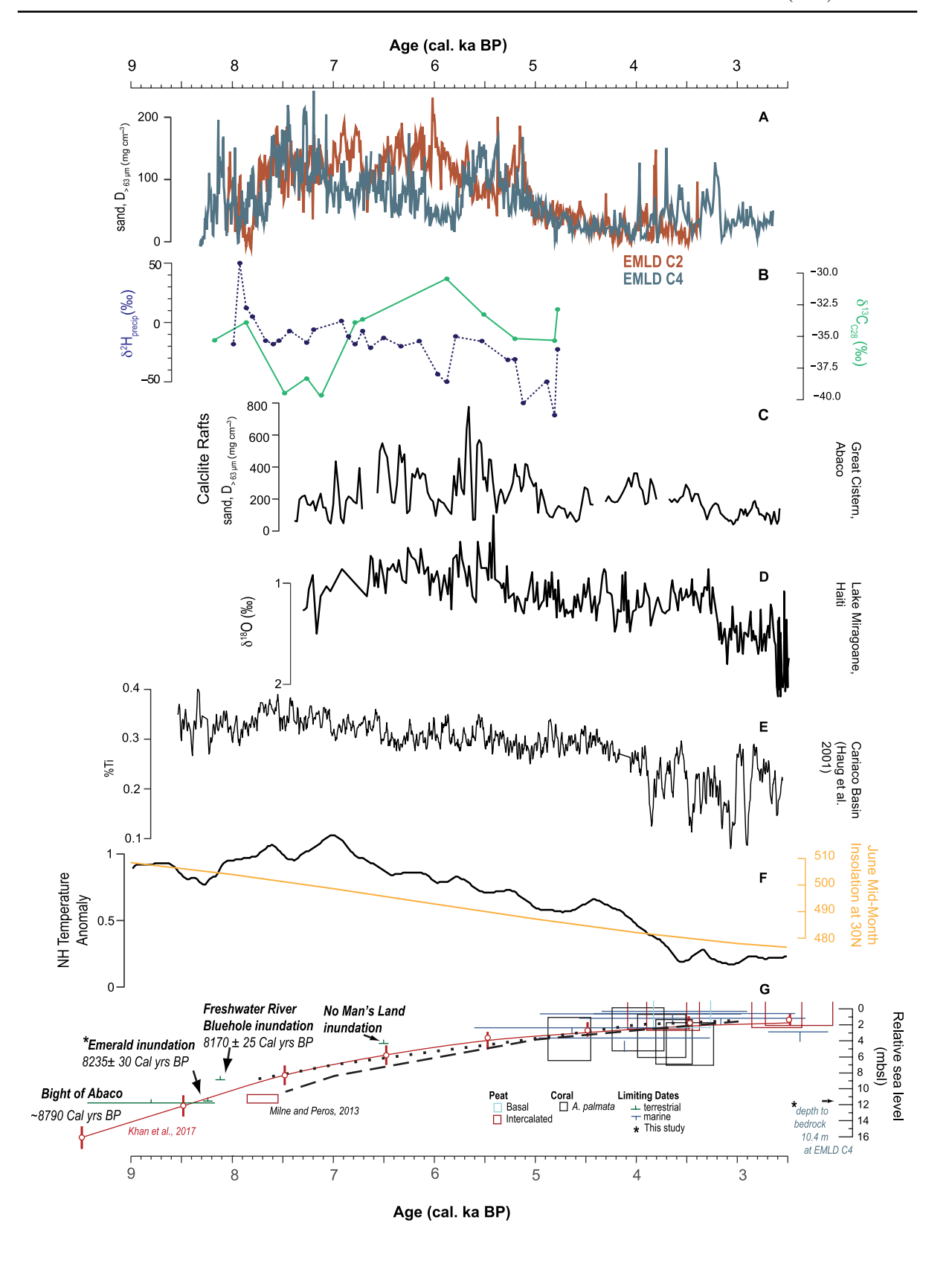
Discussion

Paleolimnology of Emerald Pond

The three primary facies of Emerald Pond (basal peat, lacustrine marl, and sapropel) have been described in other tropical North Atlantic sinkholes and lakes on carbonate landscapes, providing modern and prehistoric analogs to understand the paleolimnology in Emerald Pond. On Abaco, a lithologic transition from 'Lucayan Limestone', which is defined as 15–20% porosity and with low hydraulic conductivity of ~864 m day⁻¹ (Beach and Ginsburg 1980), to a high porosity dolostone (Holding and Allen 2015; Kaldi and Gidman 1982; Whitaker et al. 1997) occurs at 15-20 m depth. This transition marks the maximum possible vertical extent for meteoric lens development on Abaco and it is referred to in Bailey et al. (2009) as a 'Thurber Discontinuity'. Based on local sea-level indicators (van Hengstum et al. 2020a) and regional numerical estimates (Khan et al. 2017), we consider that a 'Thurber Discontinuity' in the subsurface positioned at 18-22 m should have been inundated by concomitant groundwater and sea-level rise by ~9000 years ago. As such, it is unlikely that the environmental changes in Emerald Pond that occurred over the last~8300 years were caused by a step-wise change to groundwater flow from hydraulic conductivity changes in the antecedent carbonate.

On carbonate platforms that are devoid of fluvial systems, rainwater directly infiltrates into aquifers where elevation is ultimately linked to glacio-eustatic sea-level change (Gabriel et al. 2009; Richards et al. 1994; van Hengstum et al. 2011). It is reasonable to assume that the elevation of the local water table in Emerald Pond has been just above local sea level, given that (1) the porosity of the antecedent carbonate promotes an unconfined aquifer, and (2) the minimal distance between Emerald Pond and the







√Fig. 11 Regional comparison of hydroclimate records, sea level, and North Atlantic climatic conditions. From this study: A Coarse-grained particle deposition (D>63 µm) for EMLD C2 (brown) and EMLD C4 (blue), **B** Downcore $\delta^{13}C_{28}$ from EMLD C4 (green), and reconstructed $\delta^2 H_{precip}$ (dark blue). Comparison data from the region include: C Calcite rafts from Great Cistern, Abaco (Sullivan et al. 2021), **D** δ¹⁸O values from Candona sp., an ostracode, (from Lake Miragoane, Haiti (Hodell et al. 1991b, a), E %Ti within Cariaco Basin sediments (Haug et al. 2001), F Northern to Southern Hemisphere Temperature Anomaly (Schneider et al. 2014; black line), and the mid-month (June) insolation at 30°N (orange line; Berger and Loutre 1991), and G Evidence for relative sea-level rise in the region based on indicators and resultant sea-level curve (Khan et al. 2017; Neumann and Land 1975; Rasmussen et al. 1990; van Hengstum et al. 2018, 2020a)

local shoreline would act to minimize the elevational differences imposed by local hydraulic head gradients between the ocean and the field site. However, hydraulic head can create elevational differences between the inland-groundwater table relative to sea level at the shoreline (Beddows et al. 2007; Martin et al. 2012). Therefore, basal sinkhole peats should be conservatively interpreted as terrestrial-limiting sealevel indicators. The presence of fibrous OM and low concentrations of mangrove pollen (Slayton 2010) within the basal peat provide evidence that wetland taxa (e.g., Rhizophora mangle, Laguncularia racemosa) were growing in situ in Emerald Pond. The contact between the basal peat and carbonate gravel at 8.9 m below the modern water table was dated to 8235 ± 30 (EMLD C4), which plots just above, or within uncertainty, of the relative sea-level curve for the northern Bahamas (Fig. 11G).

Basal mangrove and terrestrial peats on the epikarst surface are widely used to understand regional sea-level histories (Boardman et al. 1989; Gehrels 1999; Rasmussen et al. 1990; Törnqvist et al. 2004; Toscano and Macintyre 2003), and at worst they can provide a maximum sea-level indicator (Khan et al. 2017; Milne and Peros 2013). However, basal peats can also form in sinkhole lakes when a wetland becomes established in situ on the sinkhole talus pile (formed from initial carbonate collapse) from concomitant sea-level and the local groundwater rise since the last glacial maximum (Gabriel et al. 2009). Elsewhere on Abaco Island, in situ basal peat was found in No Man's Land (van Hengstum et al. 2018) and Freshwater River Blue Hole (van Hengstum et al. 2020a). Elsewhere in the North Atlantic,

basal sinkhole peat was also found in: Mullet Pond in Florida (Lane et al. 2011), Cenote Carwash in the Yucatan Peninsula (Gabriel et al. 2009), and a sinkhole in Grand Bahama (van Hengstum and Bernhard 2016). However, basal peat does not always develop in sinkholes, since neither Little Salt Spring (Florida) nor Cenote Jennifer (Cuba) have basal peat (Gregory et al. 2017; Peros et al. 2017; Zarikian et al. 2005). Basal peat can also be differentiated from detrital peat, OM transported from elsewhere on the adjacent epikarst surface such as in Runway Sinkhole on Great Abaco (Kovacs et al. 2013).

The stratigraphy in Emerald Pond is primarily carbonate marl, which is consistent with observations of previous sedimentologists (Shinn et al. 1996) and work elsewhere (Peros et al. 2017; van Hengstum et al. 2018). An analog site to infer the conditions that were favorable to marl deposition in Emerald Pond is based on the extensive geochemistry and sedimentology conducted at Wallywash Great Pond (WGP, $17.97^{\circ}N$, $-77.80^{\circ}E$, max, 5 m water depth, size: 0.76 km²), a groundwater-fed lake on limestone terrain in Jamaica, that has been the focus of extensive geochemical and sedimentological research (Holmes et al. 1995a, 1995b; Street-Perrott et al. 1993). This lake accumulated~3 m of lacustrine marl during the late Holocene (Holmes et al. 1995b). Marl deposition was promoted by several processes (Holmes et al. 1995a; Street-Perrott et al. 1993). First, cooler groundwater (25 °C) discharging into a warmer lake (28.5–31 °C) degasses CO₂ and raises the lake-water pH above 8 (Holmes et al. 1995a). As pH transitions above 7.5 in lakes, saturation index of calcite (SI_{calcite}) exceeds 0 and calcium-carbonate precipitation is favored (Holmes et al. 1995a). Second, in alkaline waters with pH > 8 and low $CO_{2 \text{ (aq.)}}$, submerged macrophytes (e.g., Chara, Potamogeton) can directly use HCO₃⁻ in photosynthesis. This process raises the pH of water, increases its alkalinity, and promotes CaCO₃ precipitation by increasing the SI_{calcite} (i.e., biogenic decalcification of spring water). Lacustrine marl deposition is mediated by the concentration of dissolved ions in lake water, which is impacted by (1) evaporation, (2) degassing of CO₂ of thermally distinct water bodies mixing, and (3) decalcification of freshwater through bicarbonate assimilation by submerged plants and algae.

Continuous lacustrine marl deposition from ~8300 to 1700 cal. yr BP (~6600 years) suggests an



extended period of stable hydrographic conditions in Emerald Pond. Based on the salinity tolerance of testate amoebae (0 to 3.5 psu) and the constant presence of testate amoebae in the stratigraphy, there is no evidence to suggest that salinity in Emerald Pond ever exceeded 3.5 psu during marl deposition. There are at least two hypotheses that could be driving broadscale marl precipitation in Emerald Pond from~8300 to 1700 cal. yr BP. First, air temperature at Abaco in the mid-Holocene could have been warmer, promoting a more isothermal sinkhole-water column and consistent degassing of CO₂, similar to late Quaternary conditions in Wallywash Great Pond (Holmes et al. 1995a). Second, increased rainfall and associated groundwater-flow rates (reasonably assuming that the freshwater meteoric lens on the carbonate platform is saturated with respect to HCO₃⁻) would result in consistent bicarbonate concentration, promoting assimilation by plants and algae. It is possible that these conditions are not mutually exclusive, perhaps aquatic conditions and sedimentation were both influenced by climate. However, these conditions do not exist today; recent hydrographic profiling indicates that the pH is too low, and water-column temperature near the sediment-water interface is too variable for lacustrine carbonate-marl precipitation (Fig. 3).

The salient decrease in coarse particle deposition and subtle changes in ostracod assemblages does suggest some internal environmental change over time at Emerald Pond. While the multidecadal variations in D. stevensoni and other ostracods are most likely attributable to natural patchiness in species distributions as preserved in the stratigraphic record, longterm appearance and disappearance of species is likely environmentally meaningful. In general, preserved charophyte remains (gyrogonites) are most common prior to ~6500 cal. yr BP, which indicates the sediment-water interface was at least occasionally covered with benthic green macroalgae coincident with freshwater ostracods D. stevensoni (Assemblage 1) and C. vidua (Assemblage 2) dominating the meiofauna. When the nearby sinkhole lake No Man's Land was first inundated by concomitant groundwater and Holocene sea-level rise, the first ostracod colonizers in this shallow sinkhole were D. stevensoni and C. vidua (van Hengstum et al. 2018). Elsewhere, it has been observed that D. stevensoni tolerates shallow settings (<1 m; van Hengstum and Bernhard 2016), as long as dissolved oxygen levels remain above the hypoxic boundary (> 2 mg L^{-1} ; Delorme 1970). From 6500 to 5500 cal. yr BP, C. annae and P. globulus were also present in Emerald Pond along with D. stevensoni and C. vidua. However, charophyte remains became less common (Pérez et al. 2010b) and P. globulus is considered nektobenthic, which suggests that a deepening water column perhaps favored a modest diversification in ostracods and loss of charophytes at 6500 cal. yr BP. From 5500 to 4500 cal. yr BP, ostracods were dominated by C. ilosvayi and C. annae, and there was a salient decrease in coarse particle deposition. The benthic C. ilosvayi is widespread in tropical and subtropical lakes, and C. ilosvayi (<3.2 psu; Pérez et al. 2010b) and C. annae (generally < 3 psu, but as high as 8 psu; Keyser 1977) have a slightly higher salinity tolerance than D. stevensoni (generally < 2 psu: Keyser 1977). It is possible that this subtle change in salinity and coarse particle deposition is linked to groundwater reorganization following inundation of the Bight of Abaco between 5980 to 5570 cal. yr BP (van Hengstum et al. 2020a), which would have separated the previously connected groundwater systems of Grand Bahama and Abaco Island (Gulley et al. 2016). Alternatively, perhaps a deepening water column and ongoing evaporation from the water table increased the cation concentration in the sinkhole, such that it exceeded ecological thresholds for the ostracods. Nevertheless, the ostracods appear to document long-term subtle environmental variations (e.g., water-column deepening, minor salinity shifts, habitat partitioning) in Emerald Pond at the multi-centennial timescales, as opposed to revealing multi-decadal changes in groundwater variability.

The carbonate marl to sapropel contact observed in EMLD RP5 suggests that the limnology of Emerald Pond fundamentally changed at ~1700 cal. yr BP. The deposition of sapropel suggests enhanced in situ organic carbon production or accumulation in the sinkhole, in turn leading to more organic carbon degradation, increased $\rm CO_2$, and lower pH (increased acidity). Small water-table increases (as low as <1 m) can increase primary productivity in sinkhole lakes, and resultant sapropel deposition (van Hengstum et al. 2020a). Similarly, geomorphologically deep sinkholes can experience increased light availability and in situ primary productivity when the water table approaches the subaerial surface (Gregory et al. 2017). Alternatively, slightly cooler regional conditions in the



circum North Atlantic region from ~ 1650 to 1350 cal. yr BP, which is known as the Dark Ages Cold Period (Helama et al. 2017), could have increased sinkholelake stratification and sapropel deposition independent of a change to primary productivity as increased stratification can contribute to increased oxygen consumption and OM preservation in the hypolimnion (Dean 1999). Sapropel is not a diagnostic salinity indicator since it can accumulate in sinkholes and karst lakes that are marine, e.g., Mangrove Lake, Bermuda (Hatcher et al. 1982), brackish, e.g., Yax Chen, Mexico (Gabriel 2008), or freshwater, e.g., Carwash Cave, Mexico (van Hengstum et al. 2010). However, the presence of a few ostracods (e.g., C. ilosvyi and C. annae) within the sapropel does suggest similar oligohaline salinity conditions as during marl deposition. Algal sapropel deposition ceased in Emerald Pond just after ~ 1400 cal. yr BP. This is intriguingly close to the interval when calcite-raft deposition in the nearby Great Cistern sinkhole ceased (Sullivan et al. 2021). Perhaps this coeval change in sedimentology in two sinkholes suggest a broader linkage to changing regional hydroclimate, or a response to continued Holocene sea-level rise and broader inundation of the eastern Little Bahamas Bank. Late Holocene limnologic conditions from ~ 1300 cal. yr BP until present supported slower deposition rates of lacustrine marl or sapropel than recorded earlier in the Holocene.

Plant wax evidence for hydroclimate variability

The reconstructed values from Emerald Pond align with recorded δ²H_{precip} from Centro de Protección e Higiene de la Radiación, ranging from -66.3 to 20.6% (Fig. 2), and are thus theoretically possible. However, modern seasonality of $\delta^2 H_{precip}$ ranges from -15.2 to -3.5% (Tamalavage et al. 2020), which makes the range of variability recorded in Emerald Pond sediment (~110%) surprising given the time averaging of sediments (i.e., each sample integrates ~ 8 years). There are no mangroves in the area and only a few intervals containing low concentrations of mangrove pollen (potentially from aeolian deposition) beyond higher concentrations in the basal peat (Slayton 2010). Therefore, the input of mangrove OM impacting $\delta^2 H_{leafwax}$ values is not a concern at Emerald Pond unlike at other coastal sinkholes (Tamalavage et al. 2020). Additionally, $\delta^{13}C_{28}$ values do not covary with δ^2H or in tandem with any vegetation components described in the pollen records (Slayton et al. 2010).

We therefore tentatively interpret δ^2 H values of the C₂₈ n-alkanoic acids as evidence for past precipitation, not vegetation shifts. The measured $\delta^2 H_{\text{precip}}$ values are relatively consistent from ~8000 to 6100 cal. yr BP (mean: $-13.7\%0 \pm 6\%0$), but more depleted values around (i) ~ 6000 and (ii) from 5400 to 4800 cal. yr BP (mean: $-40.1\% \pm 22\%$) suggest rainfall increased. A simultaneous decrease in the quantity of terrestrially-derived leaf waxes (Fig. 6) and accumulation or production of coarse-grained sedimentary particles and ostracods at ~ 5000 cal. yr BP (Fig. 11A) potentially suggests the proxies are linked to local precipitation on centennial timescales. There is evidence that the period prior to 5000 years ago was wetter on nearby Haiti (Hodell et al. 1991a), and stable oxygen isotopic ratios preserved in a speleothem from Cuba suggest increasing rainfall during the middle Holocene with modern rainfall regimes established by 5500 years ago (Fensterer et al. 2013). On Abaco, there is evidence for centennial-scale oscillations in precipitation during the middle to late Holocene, along with evidence for a notable shift to less rainfall occurring around 5000 years ago (Sullivan et al. 2021). In Emerald Pond, perhaps the shift in coarse particle deposition at 5100 cal. yr BP (limnological response) and shift to more depleted $\delta^2 H_{precip}$ values from 5400 to 4800 cal. yr BP (landscape response) is a local response to regional synoptic-scale hydroclimate changes occurring around this time, or related to source-water-salinity changes. However, higher resolution hydroclimate records than those presented here, ideally calibrated to the instrumental record to better resolve seasonal effects (boreal summer vs. winter), would significantly improve our understanding of regional rainfall changes during the Holocene.

Plant wax carbon isotopes provide additional information about the surrounding vegetation and possibly hydroclimate changes. More enriched $\delta^{13}C_{28}$ values occur from ~6900 to 4800 cal. yr BP, with the most enriched value (-30%) at ~6000 cal. yr BP (Fig. 11B). These enriched δ^{13} C_{28} values, which are typically attributed to OM from open canopy woodlands or conifers (Diefendorf and Freimuth 2017), are consistent with pollen evidence for a modest increase in *Pinus* and palm species on the Abaco landscape after ~6300 cal. yr BP (Slayton 2010). In addition, the $\delta^{13}C_{28}$ variability may be explained by



varied inputs of vegetation, from diverse plant communities recorded by pollen within Emerald Pond from ~7000 to 6500 cal. yr BP (Slayton 2010). $\delta^2 H$ is stable from ~6900 to 6000 cal. yr BP when $\delta^{13}C_{28}$ values shift, suggesting that $\delta^2 H_{28}$ is not perturbed by the vegetation shifts.

The timescales of the plant-wax archive are assumed to be contemporaneous with other macrofossil accumulation, however, it is possible that pre-aging impacts the preserved leaf-wax signatures through prolonged storage in soils, as has been reported in lakes draining landscapes with accumulating soils that developed in the post-glacial landscape of glaciated, continental north America (Freimuth et al. 2021). Within a similar karstic environment in the Yucatan Peninsula, with low topographic relief, compound-specific radiocarbon analyses revealed aged leaf wax n-alkanoic acids (350-1200 years older than bulk sediment; Douglas et al. 2014). They suggested long soil residence times (>50 cm) and transport to the lake through either overland transport or subterranean conduits (Douglas et al. 2014). Pre-aging of leaf waxes, i.e., the storage of plant wax on the landscape prior to remobilization and deposition, should work to smooth the original δ^2 H signal (French et al. 2018; Inglis et al. 2022). It is possible that the Emerald Pond leaf-wax record may be older from the dated terrestrial plant macrofossils upon which the age model is based (Fig. 5), if plant wax and macrofossils have different transport pathways and residence times (e.g., soil storage of plant wax), as suggested in the Douglas et al. (2014) karstic setting. However, leaves and their waxes, seeds, and other macrofossils may also have equivalent rapid input into the basin (e.g., via wind transport). In this setting, we suspect transport is rapid given (1) nearby terrestrial surface has limited soil cover (<25 cm) constraining storage times, and (2) the abrupt isotopic shifts observed in the record. Although this remains untested without costly and large sample requirements of compound-specific radiocarbon analysis, we suggest that biomarkers accumulating in Emerald Pond can be assumed to be synchronous with the organic macrofossil-age mode.

The influence of climate factors on regional hydroclimate through time

Middle to late Holocene hydroclimate change in the northern Caribbean is coeval with the decrease in northern hemisphere (NH) summer insolation (Fig. 11F). Paleoclimate reconstructions in the subtropical North Atlantic have been used to infer ITCZ behavior over centennial and millennial timescales (Haug et al. 2001; Hodell et al. 1995; Lane et al. 2011), as it is a major driver of hydroclimate variability in the Yucatan, Central America, and the northern part of the South American continent. In contrast, the NASH primarily regulates boreal summer precipitation in the subtropical North Atlantic (Li et al. 2012), but a lack of records means that NASH behavior on paleoclimate timescales is less understood. ENSO variability may further confound regional transitions between pluvial versus arid intervals (Barron and Anderson 2011; Sandweiss et al. 1996), and ENSO is a primary regulator of boreal winter rainfall in the northern Bahamas (Jury et al. 2007; Martinez et al. 2019). Given that isotope-enabled Community Earth System Model simulations suggest that ²H-depleted rainfall corresponds to a weak NASH (lower central pressure, and western boundary displaced to the East; Tamalavage et al. 2020), it is possible that δ^2 H ratios preserved in Emerald Pond document a more eastern NASH edge position from ~6000 to 4800 cal. yr BP, that in turn increased rainfall at Abaco.

Most current generation climate models suggest that the subtropical North Atlantic region should be drier (especially in boreal summer) during the middle Holocene (6000 cal. yr BP– based on PMIP4-CMIP6 simulations; Fig. 6 in Brierley et al. (2020)). This discrepancy between climate and paleoclimate data could result from a number of issues inherent to simulating the climate of the mid-Holocene in the subtropical North Atlantic. For instance, climate models underestimate the West African Monsoon extent at~6000 cal. yr BP (Braconnot et al. 2007), in part, because of issues capturing the "Green Sahara" or African Humid Period (Gasse 2000). Improved West African Monsoon simulations that include vegetation feedbacks and changes to the dust-aerosol forcing during the mid-Holocene (Pausata et al. 2016), and improved paleoclimate records (Shanahan et al. 2015;



Tierney et al. 2017) have narrowed this discrepancy. A strengthened West African Monsoon has connections to ENSO (Pausata et al. 2017) and hurricane activity (Dandoy et al. 2021) in the mid-Atlantic, both of which are likely to be relevant to Caribbean hydroclimate. The impacts of the West African Monsoon on the NASH, however, are not fully understood. Nevertheless, the strength and extent of the NH monsoons and NASH position are likely linked through stationary wave dynamics (Kelly et al. 2018; Mantsis et al. 2013). Since the NASH is a key regulator of rainfall in the subtropical North Atlantic, further work on constraining NASH behavior during the mid-Holocene, its link to the NH monsoon systems, and the role for orbital forcing in driving these changes may address the discrepancy between climate model and proxy records. Additional high-resolution sedimentary records from this region will help to inform the regional hydroclimate history and better enable spatial comparison with climate models.

Conclusions

- Emerald Pond contains a basal peat deposit (8.9 m below modern sea level) containing *Rhizophora* pollen likely formed in-situ in Emerald Pond by 8235±30 cal. yr BP at 8.9 m below modern sea level. This sea-level indicator plots within uncertainties of independent estimates for sea-level position in the early Holocene (Khan et al. 2017; Neumann and Land 1975; Rasmussen et al. 1990; van Hengstum et al. 2018, 2020a).
- From ~8300 cal. yr BP to ~1700 cal. yr BP, lacustrine marl accumulated within Emerald Pond, during a period of relatively stable limnological conditions with salinity < 3.5 psu. However, a modest internal environmental change did occur at ~5500 cal. yr BP, which was marked by decreased coarse particle deposition and ostracod faunal changes. Because of uncertainties, it is not possible to isolate whether this change was caused by synchronous hydrogeologic shifts from inundation of the Bight of Abaco on the Little Bahama Bank, or regional hydroclimate forcing in the Atlantic Ocean.</p>
- The measured δ²H of plant-wax biomarkers from surrounding vegetation are interpreted as a record of precipitation isotopic composition. While

- measured values are generally stable, oscillations to more depleted values from ~6000 to 4800 cal. yr BP may correspond to wetter conditions recorded by nearby hydroclimate records and with dynamic interpretations of a weaker NASH. However, uncertainties related to confounding effects such as changes to source water (e.g., groundwater) cannot be excluded.
- We also measured the δ^{13} C of plant wax biomarkers and see large variations that may correspond to closed canopy forest and open vegetation; however, these shifts do not align with the δ^2 H variations or pollen records and remain ambiguous.
- The limnology fundamentally changed at ~1700 cal. yr BP and ~1300 cal. yr BP, when sapropel deposition was initiated and ceased, respectively. This interval aligns closely with the Dark Ages Cold Period (e.g., 1650–1350 cal. yr BP), and perhaps reflects a local response to a period of regional cooling seasurface temperatures (Helama et al. 2017). Environmental conditions in Emerald Pond (seasonal pH range: 7.2–7.8) do not presently promote either marl or sapropel deposition as it did in the past.

Acknowledgements Field access and permissions were supported by AMMC/National Museum of The Bahamas and permits granted by The Bahamas Environment, Science and Technology (BEST) Commission. Additional coring/field support from Victoria Keeton. Sample preparation for plant-wax analyses were conducted with laboratory assistance at USC from undergraduates Efrain Vidal and Hyo Sun (Sunny) Lee. We thank Dr. Sally Horn for helpful discussions throughout the project. The manuscript was improved with the review comments of two anonymous reviewers.

Author contributions We use the formal Contributor Roles Taxonomy (CRediT) to acknowledge the work of this team. All authors contributed to the conceptualization of this work over a three-year period. AET: data curation, formal analysis, funding acquisition, investigation, project administration, supervision, validation, visualization, writing- original draft. PJH: funding acquisition, investigation, project administration, resources, supervision, visualization, writing-original draft. SJF: data curation, funding acquisition, investigation, resources, validation, writing-original draft. SC: funding acquisition, investigation, resources, writing-original draft. SNL: data curation, investigation, validation, visualization, writing-original draft. TSW: investigation, validation, writing-review and editing. RMS: formal analysis, investigation, visualization, writingreview and editing. NAA: investigation, project administration, resources, writing-review and editing. JPD: funding acquisition, validation, resources, writing review and editing. PL: funding acquisition, resources, writing review and editing.



Funding Plant wax analyses were funded by US National Science Foundation EAR-1703141 to SF, EAR-1703087 to PvH and by a 2019 Graduate Student Research Grant to AT from the Geological Society of America. Additional analytical support was funded by EAR-1702946 and AGS-1805480 to SC.

Data availability All data associated with this submission are publicly available within the NOAA Paleoclimatology repository: https://www.ncdc.noaa.gov/paleo/study/31372.

Declarations

Competing interests The authors declare no competing interests. Additionally, there are no known competing financial interests or personal relationships that could have appeared to influence the work reported in this paper.

Appendix

See Tables 1 and 2.

Table 1 Conventional radiocarbon dates for EMLD C1, C2, C3, and RP5

Accession number	Core	Section	Core section depth (cm)	Total core depth (cm)	F ¹⁴ C	Conventional ¹⁴ C age (yr)	Conventional Age Error (yrs)	δ ¹³ C (‰)
OS-152150	EMLD C1	1:3	10.5	10.5	0.9158 ± 0.0021	705	20	N/A
OS-152151	EMLD C1	1:3	49	49	0.7548 ± 0.0015	2260	15	N/A
OS-152152	EMLD C1	2:3	5.5	97.5	0.725 ± 0.0016	2580	15	N/A
OS-152153	EMLD C1	2:3	111.5	203.5	0.6455 ± 0.0017	3520	20	N/A
OS-152214	EMLD C1	3:3	101.25	317.75	0.5692 ± 0.0015	4530	20	- 25.25
OS-153819	EMLD C2	1:5	31.75	31.75	0.68 ± 0.0020	3100	25	- 27.95
OS-153820	EMLD C2	1:5	77	77	0.6445 ± 0.0018	3530	25	-27.44
OS-153792	EMLD C2	2:5	69.25	192.25	0.5955 ± 0.0114	4160	150	-30.62
OS-153821	EMLD C2	5:5	20.25	445.25	0.4388 ± 0.0019	6620	35	-25.41
OS-153793	EMLD C2	5:5	119.75	544.75	0.406 ± 0.01	7240	200	- 30.28
OS-152215	EMLD C4	1:7	14.5	14.5	0.729 ± 0.0016	2540	20	- 25.77
OS-152216	EMLD C4	1:7	49.5	49.5	0.7014 ± 0.0018	2850	20	-28.34
OS-137772	EMLD C4	2:7	2	125	0.6328 ± 0.0016	3680	20	-25.69
OS-137773	EMLD C4	2:7	37.5	160.5	0.6259 ± 0.0016	3760	20	-25.50
OS-133773	EMLD C4	2:7	71.5	194.5	0.5948 ± 0.0019	4170	25	-24.09
OS-133774	EMLD C4	3:7	59.5	276.5	0.5666 ± 0.0018	4560	25	-27.24
OS-133775	EMLD C4	4:7	126.5	410.5	0.4908 ± 0.0018	5720	30	-27.33
OS-133776	EMLD C4	5:7	117.5	542.5	0.4451 ± 0.0018	6500	35	-28.32
OS-133772	EMLD C4	6:7	83.5	646	0.3491 ± 0.0017	8450	40	-29.30
OS-137774	EMLD C4	7:7	2	653	0.4031 ± 0.0015	7300	30	-28.40
OS-133791	EMLD C4	7:7	64	715	0.3953 ± 0.002	7460	40	- 30.58
OS-153822	EMLD C4	7:7	49.5	700.5	0.3984 ± 0.0018	7390	35	- 29.25
OS-155904	EMLD RP5	1:1	5	5	0.8658 ± 0.0018	1160	15	-25.02
OS-148463	EMLD RP5	1:1	8.25	8.25	0.7429 ± 0.0016	2390	15	-25.82
OS-148464	EMLD RP5	1:1	22.5	22.5	0.8231 ± 0.0016	1560	15	-26.22
OS-148465	EMLD RP5	1:1	29.5	29.5	0.8156 ± 0.0017	1640	15	-26.92
OS-148466	EMLD RP5	1:1	49.5	49.5	0.7981 ± 0.0016	1810	15	- 29.31
OS-148467	EMLD RP5	1:1	58.75	58.75	0.7898 ± 0.0017	1900	15	-25.04
OS-155905	EMLD RP5	1:1	61.5	61.5	0.7782 ± 0.0016	2020	15	-26.22
OS-155906	EMLD RP5	1:1	54.5	54.5	0.4243 ± 0.0014	6890	25	-24.67



Table 2 Bulk coarse particle density and OM for the three main facies present within the EMLD cores

Sedimen- tary facies	Coarse particles range (mg cm ⁻³)	Coarse particles mean (mg cm ⁻³)	Bulk OM (%) range	Bulk OM (%) mean
Peat	13.7 to 28.9	21.5 ± 5.5	3.0 to 79.4	79.5 ± 3.4
Marl	5.4 to 327.1	89.0 ± 5.7	0.3 to 88.0	5.7 ± 8.1
Sapropel	11.8 to 118.1	49.2 ± 26.4	31.0 to 86.0	62.2 ± 14.3

References

- American Public Health Association (1989) Standard method for the examination of water and wastewater. In: Clesceri LS, Greenberg AE, Trussell RR (eds.), 17th ed. Washington DC.
- Arienzo MM, Swart PK, Broad K, Clemen AC, Pourmand A, Kakuk B (2017) Multi-proxy evidence of millenial climate variability from multiple Bahamian speleothems. Quat Sci Rev 161:18–29
- Bailey RT, Jenson JW, Olsen AE (2009) Numerical modeling of atoll island hydrogeology. Groundwater 47:184–196
- Barron JA, Anderson L (2011) Enhanced Late Holocene ENSO/PDO expression along the margins of the eastern North Pacific. Quat Int 235:3–12
- Beach DK, Ginsburg RN (1980) Facies succession of Pliocene-Pleistocene carbonates, northwestern Great Bahama Bank. Am Assoc Petrol Geol Bull 64:1634–1642
- Beddows PA, Smart PL, Whitaker FF, Smith SL (2007) Decoupled fresh–saline groundwater circulation of a coastal carbonate aquifer: spatial patterns of temperature and specific electrical conductivity. J Hydrol 346:18–32
- Berger A, Loutre M-F (1991) Insolation values for the climate of the last 10 million years. Quat Sci Rev 10:297–317
- Bhattacharya T, Coats S (2020) Atlantic-Pacific gradients drive last millennium hydroclimate variability in Mesoamerica. Geophys Res Lett 47:e2020GL088061
- Blaauw M, Christen JA (2011) Flexible paleoclimate age-depth models using an autoregressive gamma process. Bayesian Anal 6:457–474
- Black M (1932) VI. The algal sediments of Andros Island, Bahamas. Philos Trans R Soc Lond Ser B 222:165–192
- Boardman MR, Neumann A, Rasmussen K (1989) Holocene sea level in the Bahamas. In: Proceedings of fourth symposium on the geology of the Bahamas, Bahamian Fieldstation, Fort Lauderdale, pp. 45–52
- Braconnot P, Otto-Bliesner B, Harrison S, Joussaume S, Peterchmitt J-Y, Abe-Ouchi A, Crucifix M, Driesschaert E, Fichefet T, Hewitt C (2007) Results of PMIP2 coupled simulations of the Mid-Holocene and Last Glacial Maximum-Part 2: feedbacks with emphasis on the location of the ITCZ and mid-and high latitudes heat budget. Clim Past 3:279–296
- Brady GS, Robertson D (1870) I.—The Ostracoda and Foraminifera of Tidal Rivers. With an analysis and descriptions of the Foraminifera, by Henry B. Brady, FLS. Ann Mag Nat Hist 6:1–33
- Brierley CM, Zhao A, Harrison SP, Braconnot P, Williams CJ, Thornalley DJ, Shi X, Peterschmitt J-Y, Ohgaito R, Kaufman DS (2020) Large-scale features and evaluation of

- the PMIP4–CMIP6 midHolocene simulations. Clim Past 16:1847–1872
- Carew JL, Mylroie JE (1997) Geology of the Bahamas. In: Vacher L, Quinn T (eds) Geology and hydrogeology of carbonate islands, Developments in Sedimentology. Elsevier Science Publishers, Amsterdam, pp 91–139
- Cole LG (1910) The caverns and people of the northern Yucatan. Bull Am Geogr Soc 42:321–336
- Coutino A, Stastna M, McNeill-Jewer C, Reinhardt EG (2021) Inland tidal oscillaions within the Yucatan Peninsula. Geophys Res Lett 48:e2020GL092091
- Daday EV (1905) Untersuchungen über die Süsswassermikrofauna Paraguays. Zoologica 44
- Dandoy S, Pausata FS, Camargo SJ, Laprise R, Winger K, Emanuel K (2021) Atlantic hurricane response to Saharan greening and reduced dust emissions during the mid-Holocene. Clim Past 17:675–701
- Dean WE (1999) The carbon cycle and biogeochemical dynamics in lake sediments. J Paleolimnol 21:375–393
- Delorme LD (1970) Freshwater ostracodes of Canada: families Ilyocyprididae, Notodromadidae, Darwinuliadale, Cytherideidae, Entocytheridae (Part IV). Cand J Zool 48:1251–1259
- Diefendorf AF, Freimuth EJ (2017) Extracting the most from terrestrial plant-derived n-alkyl lipids and their carbon isotopes from the sedimentary record: a review. Org Geochem 103:1–21
- Dix GR, Patterson RT, Park LE (1999) Marine saline ponds as sedimentary archives of late Holocene climate and sealevel variation along a carbonate platform margin: Lee Stocking Island, Bahamas. Palaeogeogr Palaeoclimatol Palaeoecol 150:223–246
- Douglas PM, Pagani M, Eglinton TI, Brenner M, Hodell DA, Curtis JH, Ma KF, Breckenridge A (2014) Pre-aged plant waxes in tropical lake sediments and their influence on the chronology of molecular paleoclimate proxy records. Geochim Cosmochim Acta 141:346–364
- Escobar J, Brenner M, Whitmore TJ, Kenney WF, Curtis JH (2008) Ecology of testate amoebae (thecamoebians) in subtropical Florida lakes. J Paleolimnol 40:715–731
- Fall PL, van Hengstum PJ, Lavold-Foote L, Donnelly JP, Albury NA, Tamalavage AE (2021) Human arrival and landscape dynamics in the northern Bahamas. In: Proceedings of the National Academy of Sciences, 118
- Feakins SJ, Bentley LP, Salinas N, Shenkin A, Blonder B, Goldsmith GR, Ponton C, Arvin LJ, Wu MS, Peters T, West AJ, Martin RE, Enquist BJ, Asner GP, Malhi Y (2016) Plant leaf wax biomarkers capture gradients in hydrogen isotopes of precipitation from the Andes and Amazon. Geochim Cosmochim Acta 182:155–172



- Fensterer C, Scholz D, Hoffman DL, Spotl C, Schroder-Ritzrau A, Horn C, Pajon JM, Mangini A (2013) Millennial-scale climate variability during the last 12.5 ka recorded in a Caribbean speleothem. Earth Planet Sci Lett 361:143–151
- Ficken KJ, Li B, Swain D, Eglinton G (2000) An n-alkane proxy for the sedimentary input of submerged/floating freshwater aquatic macrophytes. Org Geochem 31:745–749
- Freeman KH, Pancost R (2014) Biomarkers for terrestrial plants and climate, 2nd ed. In: Treatise on Geochemistry
- Freimuth EJ, Diefendorf AF, Lowell TV, Schartman AK, Landis JD, Stewart AK, Bates BR (2021) Centennial-scale age offsets of plant wax n-alkanes in Adirondack lake sediments. Geochim Cosmochim Acta 300:119–136
- French KL, Hein CJ, Haghipour N, Wacker L, Kudrass HR, Eglinton TI, Galy V (2018) Millennial soil retention of terrestrial organic matter deposited in the Bengal Fan. Sci Rep 8:11997
- Furtos NC (1933) The Ostracoda of Ohio. Bull Ohio Biol Surv 29:413–492
- Furtos NC (1936) On the Ostracoda from the Cenotes of the Yucatan and vicinity. In: Pearse AS, Creaser EP, Hall FG (eds) The cenotes of the Yucatan: a zoological and hydrological survey. Carnegie Institution of Washington, Washington
- Gabriel JJ, Reinhardt EG, Peros MC, Davidson DE, van Hengstum PJ, Beddows PA (2009) Palaeoenvironmental evolution of Cenote Aktun Ha (Carwash) on the Yucatan Peninsula, Mexico and its response to Holocene sea-level rise. J Paleolimnol 42:199–213
- Gamble DW, Curtis S (2008) Caribbean precipitation: a review, model and prospect. Prog Phys Geogr 32:265–276
- Gasse F (2000) Hydrological changes in the African tropics since the last glacial maximum. Quat Sci Rev 19:189–211
- Gehrels WR (1999) Middle and late Holocene sea-level changes in eastern Maine reconstructed from foraminiferal saltmarsh stratigraphy and AMS ¹⁴C dates on basal peat. Quat Res 52:350–359
- Gregory BRB, Reinhardt EG, Gifford JA (2017) The influence of morphology on sinkhole sedimentation at Little Salt Spring, Florida. J Coast Res 33:359–371
- Grimm EC, Jacobson GL, Watts WA, Hansen BC, Maasch KA (1993) A 50,000-year record of climate oscillations from Florida and its temporal correlation with the Heinrich events. Science 261:198–200
- Gulley JD, Mayer AS, Martin JB, Bedekar V (2016) Sea level rise and inundation of island interiors: assessing impacts of lake formation and evaporation on water resources in arid climates. Geophys Res Lett 43:9712–9719
- Hatcher PG, Simoneit BR, Mackenzie FT, Neumann AC, Thorstenson DC, Gerchakov SM (1982) Organic geochemistry and pore water chemistry of sediments from Mangrove Lake, Bermuda. Org Geochem 4:93–112
- Haug GH, Hughen KA, Sigman DM, Peterson LC, Röhl U (2001) Southward migration of the intertropical convergence zone through the Holocene. Science 293:1304–1308

- Haug GH, Günther D, Peterson LC, Sigmna DM, Hughen KA, Aeschlimann B (2003) Climate and collapse of Maya civilization. Science 299:1731–1734
- Heiri O, Lotter AF, Lemcke G (2001) Loss on ignition as a method for estimating organic and carbonate content in sediments: reproducibility and comparability of results. J Paleolimnol 25:101–110
- Helama S, Jones PD, Briffa KR (2017) Dark ages cold period: a literature review and directions for future research. Holocene 27:1600–1606
- Hodell DA, Curtis JH, Jones GA, Higuera-Gundy A, Brenner M, Binford MW, Dorsey KT (1991a) Reconstruction of Caribbean climate change over the past 10,500 years. Nature 352:790–793
- Hodell DA, Curtis JH, Brenner M (1995) Possible role of climate in the collapse of Classic Maya civilization. Nature 375:391–394
- Hodell DA, Brenner M, Curtis JH, Guilderson T (2001) Solar forcing of drought frequency in the Maya Lowlands. Science 292:1367–1370
- Hodell DA, Brenner M, Curtis JH, Gonzalez-Medina R, Can EIC, Guilderson TP (2005) Climate change on the Yucatan Peninsula during the little ice age. Quat Res 63:109–121
- Holding S, Allen DM (2015) From days to decades: numerical modelling of freshwater lens response to climate change stressors on small low-lying islands. Hydrol Earth Syst Sci 19:933–949
- Holmes JA (1997) Recent non-marine Ostracoda from Jamaica, West Indies. J Micropalaeontol 16:137–143
- Holmes JA (1998) A late Quaternary ostracod record from Wallywash Great Pond, a Jamaican marl lake. J Paleolimnol 19:115–128
- Holmes J, Street-Perrott F, Darbyshire D, Davies N, Hales P (1995a) Chemical and isotopic composition of karstic lakes in Jamaica, West Indies. Hydrobiologia 312:121–138
- Holmes JA, Street-Peffott FA, Ivanovich M, Peffott RA (1995b) A late Quaternary palaeolimnological record from Jamaica based on trace-element chemistry of ostracod shells. Chem Geol 124:143–160
- IAEA/WMO (2019) Global network of isotopes in precipitation. The GNIP Database.
- Inglis GN, Bhattacharya T, Hemingway JD, Hollingsworth EH, Feakins SJ, Tierney JE (2022) Biomarker approaches for reconstructing terrestrial environmental change. Annu Rev Earth Planet Sci 50:369–394
- Jury M, Malmgren BA, Winter A (2007) Subregional precipitation climate of the Caribbean and relationships with ENSO and NAO. J Geophys Res Atmos. https:// doi.org/10.1029/2006JD007541
- Kaldi J, Gidman J (1982) Early diagenetic dolomite cements; examples from the Permian Lower Magnesian Limestone of England and the Pleistocene carbonates of the Bahamas. J Sediment Res 52:1073–1085
- Kelly P, Kravitz B, Lu J, Leung LR (2018) Remote drying in the North Atlantic as a common response to precessional changes and CO₂ increase over land. Geophys Res Lett 45:3615–3624
- Keyser D (1975) Ostracoden aus den Mangrovegebieten von Südwest-Florida. Abhandlungen und Verhandlungen



- des Naturwissenschaftlichen Vereins in Hamburg 18(19):255–290
- Keyser D (1977) Ecology of zoogeography of recent brackish-water Ostracoda (Crustacea) from south-west Florida. In: Löffler H, Danielopol D (eds) Aspects of the ecology and zoogeography of recent and fossil ostracoda. Dr. W. Junk Publishers, The Hague, pp 207–222
- Keyser D, Schöning C (2000) Holocene ostracoda (crustacea) from Bermuda. Senckenb Lethaea 80:567–591
- Keyser D (1978) Ostracoda (Crustacea) from South-West Florida. In: Aspects of ecology and zoogeography of recent and fossil Ostracoda, 207
- Khan NS, Ashe E, Horton BP, Dutton A, Kopp RE, Brocard G, Engelhart SE, Hill DF, Peltier W, Vane CH (2017) Drivers of Holocene sea-level change in the Caribbean. Quat Sci Rev 155:13–36
- Kjellmark E (1996) Late Holocene climate change and human disturbance on Andros Island, Bahamas. J Paleolimnol 15:133–145
- Kovacs SE, van Hengstum PJ, Reinhardt EG, Donnelly JP, Albury NA (2013) Late Holocene sedimentation and hydrologic development in a shallow coastal sinkhole on Great Abaco Island, The Bahamas. Quat Int 317:118–132
- Krutak PR (1971) The Recent Ostracoda of Laguna Mandinga, Veracruz, Mexico. Micropaleontology 17:1–30
- Lane CS, Horn SP, Mora CI, Orvis KH (2009) Late-Holocene paleoenvironmental change at mid-elevation on the Caribbean slope of the Cordillera Central, Dominican Republic: a multi-site, multi-proxy analysis. Quat Sci Rev 28:2239–2260
- Lane P, Donnelly JP, Woodruff JD, Hawkes AD (2011) A decadally-resolved paleohurricane record archived in the late Holocene sediments of a Florida sinkhole. Mar Geol 287:14–30
- Lane CS, Horn SP, Kerr MT (2014) Beyond the Mayan lowlands: impacts of the terminal classic drought in the Caribbean Antilles. Quat Sci Rev 86:89–98
- Lee H, Feakins SJ, Lu Z, Schimmelmann A, Sessions AL, Tierney JE, Williams TJ (2017) Comparison of three methods for the methylation of aliphatic and aromatic compounds. Rapid Commun Mass Spectrom 31:1633–1640
- Legendre P, Legendre L (1998) Developments in environmental modelling. Numer Ecol 20:1e853
- Leng MJ, Jones MD, Frogley MR, Eastwood WJ, Kendrick CP, Roberts CN (2010) Detrital carbonate influences on bulk oxygen and carbon isotope composition of lacustrine sediments from the Mediterranean. Glob Planet Change 71:175–182
- Li W, Li L, Fu R, Deng Y, Wang H (2011) Changes to the North Atlantic subtropical high and its role in the intensification of summer rainfall variability in the southeastern United States. J Clim 24:1499–1506
- Li L, Li W, Kushnir Y (2012) Variation of the North Atlantic subtropical high western ridge and its implication to Southeastern US summer precipitation. Clim Dyn 39:1401–1412
- Little SN, van Hengstum PJ (2019) Intertidal and subtidal benthic foraminifera in flooded caves: implications for

- reconstructing coastal karst aquifers and cave paleoenvironments. Mar Micropaleontol 149:19–34
- Little SN, van Hengstum PJ, Beddows PA, Donnelly JP, Winkler TS, Albury NA (2021) Unique habitat for benthic foraminifera in subtidal blue holes on carbonate platforms. Front Ecol Evol 9:951
- Mackinnon L, Jones B (2001) Sedimentological evolution of North Sound, Grand Cayman-a freshwater to marine carbonate succession driven by Holocene sea-level rise. J Sediment Res 71:568–580
- Mantsis DF, Clement AC, Kirtman B, Broccoli AJ, Erb MP (2013) Precessional cycles and their influence on the North Pacific and North Atlantic summer anticyclones. J Clim 26:4596–4611
- Martin JB, Gulley J, Spellman P (2012) Tidal pumping of water between Bahamian blue holes, aquifers, and the ocean. J Hydrol 416–417:28–38
- Martinez C, Goddard L, Kushnir Y, Ting M (2019) Seasonal climatology and dynamical mechanisms of rainfall in the Caribbean. Clim Dyn 53:825–846
- Méhes G (1914) Süsswasser-Ostracoden aus Columbien und Argentinien. Mémoires De La Société Naturelle De Neuchâtel 5:639–663
- Milne GA, Peros M (2013) Data-model comparison of Holocene sea-level change in the circum-Caribbean region. Glob Planet Change 107:119–131
- Müller OF (1776) Zoologiae Danicae Prodomus, seu Animalium Daniae et Norvegiae indigenarum. Havniae, typis Hallagerii 274.
- Mylroie JE, Carew JL, Vacher HL (1995) Karst development in the Bahamas and Bermuda. In: Curran HA, White B (eds) Terrestrial and shallow marine geology of the Bahamas and Bermuda. Geologic Society of America, Boulder, pp 251–267
- Mylroie JEC, James L, Moore AI (1995b) Blue holes: definition and genesis. Carbonates Evaporites 10:225–233
- Neumann AC, Land LS (1975) Lime mud deposition and calcareous algae in the Bight of Abaco, Bahamas; a budget. J Sediment Res 45:763–786
- Noble RS, Curran HA, Wilson MA (1995) Paleoenvironmental and paleoecologic analyses of a Pleistocene mollusc-rich lagoonal facies, San Salvador Island, Bahamas. In: Allen H, White B (eds) Terrestrial and shallow marine geology of bahamas and bermuda. The Geological Society of America, Boulder, pp 91–103
- Oksanen J, Blanchet FG, Friendly M, Kindt R, Legendre P, McGlinn D, Minchin PR, O'Hara R, Simpson G, Solymos P (2020) vegan: community ecology package. R package version 2.5–6. 2019.
- Park LE (2012) Comparing two long-term hurricane frequency and intensity records from San Salvador Island, Bahamas. J Coast Res 28:891–902
- Park Boush LE, Myrbo A, Michelson A (2014) A qualitative and quantitative model for climate-driven lake formation on carbonate platforms based on examples from the Bahamian archipelago. Carbonates Evaporites 29:409–418
- Pausata FS, Messori G, Zhang Q (2016) Impacts of dust reduction on the northward expansion of the African monsoon during the Green Sahara period. Earth Planet Sci Lett 434:298–307



- Pausata FS, Zhang Q, Muschitiello F, Lu Z, Chafik L, Niedermeyer EM, Stager JC, Cobb KM, Liu Z (2017) Greening of the Sahara suppressed ENSO activity during the mid-Holocene. Nat Commun 8:1–12
- Pełechaty M, Pukacz A, Apolinarska K, Pełechata A, Siepak M (2013) The significance of *Chara* vegetation in the precipitation of lacustrine calcium carbonate. Sedimentology 60:1017–1035
- Pérez L, Lorenschat J, Brenner M, Scharf B, Schwalb A (2010a) Extant freshwater ostracodes (Crustacea: Ostracoda) from Lago Petén Itzá, Guatemala. Int J Trop Biol 58:871–895
- Pérez L, Lorenschat J, Bugja R, Brenner M, Scharf BS, Schwalb A (2010b) Distribution, diversity and ecology of modern freshwater ostracodes (Crustacea), and hydrochemical characteristics of Lago Petén Itzá, Guatemala. J Limnol 69:146–159
- Peros M, Collins S, Agosta G'Meiner A, Reinhardt E, Pupo FM (2017) Multistage 8.2 kyr event revealed through high-resolution XRF core scanning of Cuban sinkhole sediments. Geophys Res Lett 44:7374–7381
- R Core Team (2021) A language and environment for statistical computing. R Foundation for Statistical Computing, Vienna, Austria.
- Rasmussen KA, Haddad RI, Neumann AC (1990) Stableisotope record of organic carbon from an evolving carbonate banktop, Bight of Abaco, Bahamas. Geology 18:790–794
- Reimer PJ, Austin WE, Bard E, Bayliss A, Blackwell PG, Ramsey CB, Butzin M, Cheng H, Edwards RL, Friedrich M et al. (2020) The IntCal20 Northern Hemisphere radiocarbon age calibration curve (0–55 cal kBP). Radiocarbon 62:725–757
- Richards DA, Smart PL, Edwards RL (1994) Maximum sea levels for the last glacial period from U-series ages of submerged speleothems. Nature 367:357–360
- Roe HM, Patterson RT (2006) Distribution of thecamoebians (testate amoebae) in small lakes and ponds, Barbados, West Indies. J Foramin Res 36:116–134
- Sandweiss DH, Richardson JB, Reitz EJ, Rollins HB, Maasch KA (1996) Geoarchaeological evidence from Peru for a 5000 years BP onset of El Niño. Science 273:1531–1533
- Schneider T, Bischoff T, Haug GH (2014) Migrations and dynamics of the intertropical convergence zone. Nature 513:45–53
- Schnurrenberger D, Russell J, Kelts K (2003) Classification of lacustrine sediments based on sedimentary components. J Paleolimnol 29:141–154
- Shanahan TM, McKay NP, Hughen KA, Overpeck JT, Otto-Bliesner B, Heil CW, King J, Scholz CA, Peck J (2015) The time-transgressive termination of the African Humid Period. Nat Geosci 8:140–144
- Sharpe RW (1908) A further report on the Ostracoda of the United States National Museum. In: Proceedings of the United States National Museum.
- Shinn EA, Reich CD, Locker SD, Hine AC (1996) A giant sediment trap in the Florida Keys. J Coast Res 7:953–959
- Slayton IA (2010) A vegetation history from Emerald Pond, Great Abaco Island, the Bahamas, based on pollen analysis.

- Soulié-Märsche I (2008) Charophytes, indicators for low salinity phases in North African sebkhet. J Afr Earth Sc 51:69–76
- Soulié-Märsche I, García A (2015) Gyrogonites and oospores, complementary viewpoints to improve the study of the charophytes (Charales). Aquat Bot 120:7–17
- Steadman DW, Albury NA, Maillis P, Mead JI, Slapcinsky J, Krysko KL, Singleton HM, Franklin J (2014) Late-Holocene faunal and landscape change in the Bahamas. Holocene 24:220–230
- Street-Perrott FA, Hales PE, Perrott RA, Fontes JC, Switsur VR, Pearson A (1993) Late Quaternary paleolimnology of a tropical marl lake: Wallywash Great Pond, Jamaica. J Paleolimnol 9:3–22
- Sullivan RM, van Hengstum PJ, Coats SJ, Donnelly JP, Tamalavage AE, Winkler TS, Albury NA (2021) Hydroclimate dipole drives multi-centennial variability in the Western Tropical North Atlantic Margin during the middle and late holocene. Paleoceanogr Paleoclimatol 36:e2020PA004184
- Swain FM (1955) Ostracoda of San Antonio Bay, Texas. J Paleontol 29:561-646
- Tamalavage AE, van Hengstum PJ, Louchouarn P, Fall PL, Donnelly JP, Albury NA, Coats S, Feakins SJ (2020) Plant wax evidence for precipitation and vegetation change from a coastal sinkhole lake in the Bahamas spanning the last 3000 years. Org Geochem 150:104120
- Teeter J (1980) Ostracoda of the lake flirt formation (Pleistocene) of southern Florida. Micropaleontology 26:337–355
- Teeter JW (1989) Holocene salinity history of the saline lakes of San Salvador Island, Bahamas. In: Pleistocene and Holocene carbonate environments on San Salvador Island, Bahamas: International Geological Congress, 28th, Washington, Field Trip Guidebook T. Wiley Online Library, pp. 35–40
- Teeter JW (1995) Holocene saline lake history, San Salvador Island, Bahamas. In: Curan HA, White B (eds) Terrestrial and shallow marine geology of the Bahamas and Bermuda, pp. 117–124.
- Tierney JE, Pausata FSR, deMenocal PB (2017) Rainfall regimes of the Green Sahara. Sci Adv 3:e1601503
- Toscano MA, Macintyre IG (2003) Corrected western Atlantic sea-level curve for the last 11,000 years based on calibrated 14 C dates from Acropora palmata framework and intertidal mangrove peat. Coral Reefs 22:257–270
- Törnqvist TE, González JL, Newsom LA, Van der Borg K, De Jong AF, Kurnik CW (2004) Deciphering Holocene sea-level history on the US Gulf Coast: a high-resolution record from the Mississippi Delta. Geol Soc Am Bull 116:1026–1039
- van Hengstum PJ, Bernhard JM (2016) A new species of benthic foraminifera from an inland Bahamian carbonate marsh. J Foraminifer Res 46:193–200
- van Hengstum PJ, Reinhardt EG, Beddows PA, Huang RJ, Gabriel JJ (2008) Thecamoebians (testate amoebae) and foraminifera from three anchialine cenotes in Mexico: low salinity (1.5 4.5 psu) faunal transitions. J Foramin Res 38:305–317
- van Hengstum PJ, Reinhardt EG, Beddows PA, Gabriel JJ (2010) Linkages between Holocene paleoclimate and



- paleohydrogeology preserved in a Yucatan underwater cave. Quat Sci Rev 29:2788–2798
- van Hengstum PJ, Scott DB, Gröcke DR, Charette MA (2011) Sea level controls sedimentation and environments in coastal caves and sinkholes. Mar Geol 286:35–50
- van Hengstum PJ, Donnelly JP, Fall PL, Toomey MR, Albury NA, Kakuk B (2016) The intertropical convergence zone modulates intense hurricane strikes on the western North Atlantic margin. Sci Rep 6:1–10
- van Hengstum PJ, Maale G, Donnelly JP, Albury NA, Onac BP, Sullivan RM, Winkler TS, Tamalavage AE, Mac-Donald D (2018) Drought in the northern Bahamas from 3300 to 2500 years ago. Quat Sci Rev 186:169–185
- van Hengstum PJ, Winkler TS, Tamalavage AE, Sullivan RM, Little SN, Donnelly JP, Albury NA (2020) Holocene sedimentation in a blue hole surrounded by carbonate tidal flats in The Bahamas: autogenic versus allogenic processes. Mar Geol 419:106051
- Van Morkhoven FPCM (1963) Post-palaeozoic ostracoda: their morphology, taxonomy, and exonomic use, volume 2: generic descriptions. Elsevier Publishing Company, Amsterdam
- Walker LN, Mylorie JE, Walker AD, Mylroie JR (2008) The caves of Abaco Island, Bahamas: keys to geologic timescales. J Cave Karst Stud 70:108–119
- Wallace E, Donnelly J, van Hengstum P, Wiman C, Sullivan R, Winkler T, d'Entremont N, Toomey M, Albury N (2019) Intense hurricane activity over the past 1500 years at South Andros Island, The Bahamas. Paleoceanogr Paleoclimatol 34:1761–1783

- Whitaker D, Christman M (2014) Clustsig: significant cluster analysis. R package version 1.
- Whitaker FF, Smart PL, Vacher HL, Quinn TM (1997) Hydrogeology of the Bahamian Archipelago, pp. 183–216
- Whitaker FF, Smart PL (1997) Hydrogeology of Bahamian archipelago. In: Vacher HL, Quinn TM (eds) Geology and hydrogeology of carbonate islands: developments in sedimentology 54. Elsevier Science Publishers, Amsterdam, pp 183–216
- Winkler TS, van Hengstum PJ, Donnelly JP, Wallace EJ, Sullivan RM, Albury NA (2020) Revising evidence of hurricane strikes on Abaco Island (The Bahamas) over the last 700 years. Sci Rep 10:16556
- Zarikian CAA, Swart PK, Gifford JA, Blackwelder PL (2005) Holocene paleohydrology of little salt spring, Florida, based on ostracod assemblages and stable isotopes. Palaeogeogr Palaeoclimatol Palaeoecol 225:134–156

Publisher's Note Springer Nature remains neutral with regard to jurisdictional claims in published maps and institutional affiliations.

Springer Nature or its licensor (e.g. a society or other partner) holds exclusive rights to this article under a publishing agreement with the author(s) or other rightsholder(s); author self-archiving of the accepted manuscript version of this article is solely governed by the terms of such publishing agreement and applicable law.

